Cleaning insoluble viscoplastic soil layers using static and moving coherent impinging water jets

Fernandes, R.R., Oevermann, D.* and Wilson, D.I†

Department of Chemical Engineering and Biotechnology, Philippa Fawcett Drive, Cambridge, CB3 0AS, UK

*TU Dresden, Faculty of Mechanical Science and Engineering, Institute of Natural Materials Technology, Bergstraße 120, 01062 Dresden, Germany

Submitted to

Chem. Eng. Sci

May 2019

†Corresponding author

D. Ian Wilson

Department of Chemical Engineering and Biotechnology

Philippa Fawcett Drive

Cambridge

CB3 0AS

UK

E-mail diw11@cam.ac.uk

Abstract

Impinging liquid jets are widely employed in cleaning operations to remove residual soiling layers from walls and other surfaces of process vessels. Insoluble viscoplastic soiling layers represent challenging soils to clean as removal is primarily by hydraulic forces. The rheological behaviour of a commercial petroleum jelly was investigated and shown to exhibit significant creep below its critical stress. The removal of thin (< 1 mm) layers of petroleum jelly from glass and Perspex surfaces by coherent water jets impinging normally on vertical walls were studied experimentally. The jet clears a roughly circular area, forming a berm of removed material at the cleaning front. The shape of the berm was measured and found to depend on the ratio of the height of the water film and the initial thickness of the soil layer. The data were compared with the adhesive removal of viscoplastic soils proposed by Glover *et al.* (*J. Food Eng*., 2016, **178**, 95-109) with the momentum flow rate calculated using the results in Bhagat and Wilson (*Chem. Eng. Sci*, 2019, **152**, 606-623). The asymptotic approach to a cleaning limit observed in experiments with static nozzles required modification of the model: a semi-empirical term which represents the transition to a creeping regime is presented. The modified model allowed results obtained using static nozzles to predict the shape of the region cleaned by a jet from a similar nozzle moving across a soiled plate. The influence of process conditions on model parameters is discussed.

Keywords: Cleaning, impinging jet, viscoplastic fluid, moving jet, modelling

1. Introduction

Cleaning is an essential step in modern fast-moving consumer goods (FMCG) manufacturing, both to avoid cross-contamination of products and to remove fouling layers which can compromise product quality and hygiene. Cleaning-in-place (CIP) operations using impinging liquid jets are often employed to remove residual product layers or fouling deposits from vessel walls because they usually clean faster and require smaller volumes of liquid over traditional *fill and soak* methods (Glover *et al*., 2016).

The design of such systems depends on the nature of the material to be removed (henceforth referred to as the soil), on its response to being contacted with the liquid, and on the substrate. The liquid employed varies with the application: whilst aqueous solutions are standard in the food industry, organic solvents are likely to be employed in the pharmaceutical

and fine chemicals sectors. Fryer and Asteriadou (2009) characterised soils in terms of their reactivity towards the liquid, whilst Bhagat *et al*. (2017) proposed a characterization of cleaning mechanisms based on the mobility of the soil, *i.e*. its response to the forces imposed by a flow and thus its rheology (bulk, cohesive response) and tribology (the interactions at the soil/substrate interface). Newtonian liquids (*e.g*. oils) are examples of mobile soils, the removal of which has been studied by several workers (*e.g*. Yeckel and Middleman, 1987; Mickaily and Middleman, 1993). Non-Netwonian liquids exhibit more complex behaviour, resulting from the coupling of stresses between the cleaning liquid and the soil: Fuller and co-workers have investigated the cleaning behaviour of shear-thinning (Walker *et al*., 2012) and viscoelastic (Tsu et al., 2011) layers, respectively, subject to impinging jets. For immobile soils Bhagat *et al*. differentiated between adhesive failure, where cleaning involved breaking of the soil/substrate bonds (peeling, reported for brittle dried suspension layers by Oevermann *et al*. 2019) and cohesive failure, where shear stress wears the soil layer away (Murcek *et al*., 2019) Exposure of the soil layer to cleaning solution (*e.g*. soaking, Chee *et al*. 2019) can convert it from an immobile to a mobile form, the dynamics of which are important factors for cleaning agent selection. Soils which do not interact with the liquid and which are not mobile are therefore difficult to clean.

Viscoplastic fluids are materials which require the imposed stress to exceed some critical value before they flow (Ewoldt *et al*., 2010). Viscoplastic soils are therefore not removed simply by contact with a cleaning solution: the solution has to exert a certain force (or shear stress) before the soil will become mobile. This critical value is referred to in much of the literature as the yield stress (e.g. Barnes, 1999; Dinkgreve *et al*., 2018), noting that the understanding of the elastic-viscous transition has increased markedly in recent years. The term critical stress, τ_c, is used here for the shear stress at the transition between the elastic and viscous regimes. This paper considers the cleaning of layers of petroleum jelly, a viscoplastic material (Park and Song, 2010), from flat surfaces by a coherent impinging water jet. The petroleum jelly is hydrophobic, and so dissolution or weakening of the soil by the water can be neglected. It therefore represents a model material for studying the cleaning of viscoplastic soils, as well as presenting real challenges in some industrial sectors such as pharmaceuticals, where white soft paraffin is used as the base for balms and ointments (Rodgers *et al*., 2019). The rheological behaviour of the petroleum jelly was investigated using oscillatory and steady shear testing. Like many other notionally viscoplastic materials (Dinkgreve *et al*., 2018), it exhibits a solid-liquid transition at a critical shear stress (Coussot *et al*., 2002).

Cleaning by impinging liquid jets has been the subject of increasing attention in recent years (Wilson *et al.*, 2014; Köhler *et al.*, 2015; Feldung Damkjær *et al.*, 2017; Murcek *et al.*, 2019; Rodgers *et al.*, 2019; Yang *et al.*, 2019). This has been accompanied by quantitative understanding of the flow patterns involved and modelling of cleaning dynamics (e.g. Bhagat and Wilson, 2016). When a coherent liquid jet of radius r_o impinges on a flat surface, the liquid spreads radially away from the stagnation point until it reaches a point where the thickness of the film, h, increases sharply due to the balance of momentum, surface tension and viscous forces (Bhagat *et al.*, 2018). The hydrodynamics of the film in this radial flow zone (RFZ), located between the jet footprint (radius of order r_o) and the hydraulic jump radius r_j, was first described by Watson (1964).

Yeckel and Middelman (1987) used Watson's description to construct a model for shear-driven removal which they applied to the cleaning of thin Newtonian oil layers, *i.e.* mobile soils. Wilson *et al.* (2014) subsequently presented a model describing adhesive removal, where the momentum imposed by the liquid film causes the soil to peel away from the substrate. They postulated that the rate of growth of the circular cleaned region with radius a created by a jet impinging normally on to a soiled surface is proportional to the flow of momentum flow rate per unit length, M, *viz*.

$$\frac{da}{dt} = k'M \qquad [1]$$

where t is time and k' is a cleaning rate constant. They reported good agreement with experimental data for Xanthan gum and polyvinylacetate layers. They evaluated M using a simplified hydrodynamic description based on a parabolic velocity profile in the liquid film (see Wilson *et al.*, 2012). Bhagat and Wilson (2016) recently provided a detailed hydrodynamic description of the flow in the thin film generated when a coherent turbulent jet impinges on a vertical wall, considering the growth of a boundary layer, followed by a laminar flow zone and then possibly a turbulent region before reaching the hydraulic jump. Bhagat *et al.* (2017) showed that the evolution in the hydrodynamics results in a transition in cleaning behaviour from $a \propto t^{1/2}$ close to the point of impingement to the point where the boundary layer reaches the free surface, r_b (which they labelled 'strong soil' behaviour), to $a \propto t^{1/5}$ at longer distances (which they labelled 'weak soil'). Oevermann *et al.* (2019) demonstrated that these models gave a very good description of the experimental results of Kaye *et al.* (1995) for adhesive removal of dried suspension layers by water jets featuring velocities up to 40 m s^{-1}. They also demonstrated that the model described removal by traversing jets.

Glover *et al.* (2016) extended this approach to the cleaning of viscoplastic soil layers, investigating the cleaning of petroleum jelly by jets generated using static and moving nozzles. The existence of the critical stress resulted in the growth of the cleaned region exhibiting an asymptotic behaviour: at some radius, the force imposed by the film was not sufficient to make the soil flow. They modified Eq. [1] by including a term representing the momentum flow rate required for the soil to yield, M_{y}, giving:

$$\begin{aligned} \frac{\mathrm{d}a}{\mathrm{d}t} &= k'\left(M - M_{\mathrm{y}}\right) \qquad M > M_{\mathrm{y}} \\ \frac{\mathrm{d}a}{\mathrm{d}t} &= 0 \qquad\qquad\qquad M \leq M_{\mathrm{y}} \end{aligned} \qquad [2]$$

where M_{y} is the momentum flow rate required to yield the soil layer. They related the maximum cleaned radius, a_{max}, at a given jet flow rate to the initial thickness of the soil layer, δ_{o}, and the yield stress, τ_{y}, by modelling the shape of the soil as a wedge with angle of inclination χ to the substrate surface, giving

$$M_y = \frac{\tau_{\mathrm{c}}\delta_{\mathrm{o}}}{(\tan\chi - \sin\chi)} \qquad [3]$$

This feature was not verified experimentally. Here, we employ the notation τ_{c} since the relationship between this parameter and τ_{y} is not confirmed.

This paper presents an experimental investigation of the cleaning of a similar hydrophobic viscoplastic material, a commercial petroleum jelly. The shape of the cleaning front at different stages during cleaning is determined experimentally and insights into the mechanism are discussed. The validity of the adhesive removal model, Equation [2], is investigated using the expressions for *M* reported by Bhagat and Wilson (2016). Investigation of the cleaned region indicated that a thin film of the hydrophobic soil remained on the substrate, so removal was not truly by adhesive detachment. The experimental data indicate that Equation [2] does not provide an accurate description of removal and so a revised model is proposed. The parameters obtained by fitting the revised model to data generated for cleaning by jets from static nozzles are discussed. The usefulness of the revised model is demonstrated by its ability to describe the cleaning of similar layers by jets from moving nozzles.

2. Models

2.1 Hydrodynamic description

Following Watson (1964), the Bhagat and Wilson (2016) model divides the flow pattern into three regions:

(i) a boundary layer formation zone, extending from $r_o = d_N/2$ to r_b

$$\frac{r_b}{d_N} = 0.24 Re_j^{1/3} \quad [4]$$

(ii) laminar film zone, for $r_b < r \leq r_t$

$$\frac{r_t}{d_N} = 0.2964 Re_j^{1/3} \quad [5]$$

(iii) turbulent region, $r_t < r < r_j$

where Re_j is the jet Reynolds number ($Re_j = \rho U_o d_N/\mu$), with U_o the mean velocity and d_N the diameter of the jet (taken to be that of the nozzle), ρ the liquid density, μ its viscosity and r_j the location of the hydraulic jump. All the jets considered here were turbulent. It should be noted that the jump could occur before r_t is reached.

Table 1 summarises the model predictions for the mean velocity U, the film thickness h and M. The latter quantity is calculated from

$$M = \int_0^h \rho u^2 dz \quad [18]$$

where u is the local velocity in the radial direction and z is the co-ordinate normal to the substrate.

Table 1 also reports the corresponding expressions obtained for the Wilson *et al.* (2012) model, where the flow was modelled as a simple Nusselt film with a parabolic velocity profile. The mean velocity result is given by Eq. [15], in which U decreases from U_o with increasing r (see Figure 1). Bhagat *et al.* (2017) proposed three different scenarios which allowed simplified expressions for U (and thus M) to be combined with Eqn. [1] to yield analytical expressions for the evolution of a:

(i) 'strong' soil, at small a (close to the impinging point). A 'strong soil' is one that is removed slowly so experiments, unless conducted for long times, will feature small values of a and $U \approx U_o$. This gives

$$M = \frac{3\dot{m}}{5\pi}\frac{U_\mathrm{o}}{a} \quad [19]$$

(ii) 'weak' soil, where the soil is removed quickly and the initial behaviour is difficult to capture. Data will tend to feature large values of a, where $\frac{1}{U} \gg \frac{1}{U_\mathrm{o}}$, and this gives

$$M = \frac{3\dot{m}^3}{5\pi c}\frac{1}{a^4} \quad [20]$$

where c is a group of liquid properties ($c = 10\pi^2\rho\mu/3$).

(iii) 'intermediate' soil, in which the full form of Eq. [15] is retained and

$$M = \frac{3\dot{m}U_\mathrm{o}}{5\pi}\frac{1}{a(A + Ba^3)} \quad [21]$$

where $A = 1 - \frac{10\pi\mu}{3\dot{m}}r_0$ and $B = \frac{10\pi\mu}{3\dot{m}}\frac{1}{r_0^2}$.

Figure 1 presents the estimates of U and M obtained with the Bhagat and Wilson (2016) model, Eq. [8], [11] and [14], alongside the results for U and M for the 'strong', 'weak' and 'intermediate' soil formulations given by Eq. [19], [20] and [21], respectively, for a set of experimental conditions representative of those used in this work. As shown in Figure 1 (a), the strong soil model assumes that $U = U_\mathrm{o}$ within the boundary layer formation zone. The weak soil model – which was used to describe the hydrodynamics by Glover *et al.* (2016) – applies after the boundary layer reaches the free surface. Both the strong and weak soil models fail to describe U well in the vicinity of r_b compared to the intermediate and Bhagat and Wilson (2016) models. The weak soil formulation also overestimates M for $r < r_\mathrm{b}$, see Figure 1 (b), indicating that it does not give a reliable description of the early stages of cleaning. Both the strong and intermediate soil formulations provide estimates for M that are comparable to the more accurate estimation provided by Bhagat and Wilson (2016). The advantage of these expressions is that they yield analytical or semi-analytical (for the intermediate soil case) expressions for the evolution of the cleaning front with time (Section 2.2) and tractable results for the shape of the region cleared by a traversing jet (Section 2.3).

2.2 Cleaning of viscoplastic soil, static nozzle

(i) 'Weak soil' case: $r_\mathrm{b} < a_\mathrm{max} < r_\mathrm{j}$

Glover *et al.* (2016) considered the case where M is given by Equation [20], which arises when k' is large so that initial soil removal is fast. Cleaning stops when $M = M_y$, at radial distance a_{max}, hence

$$M_y = \frac{3\dot{m}^3}{5\pi c}\frac{1}{a_{max}^4} \quad [22]$$

Eq. [2] can then be written

$$\frac{da}{dt} = k'\frac{3\dot{m}^3}{5\pi c}\left(\frac{1}{a^4} - \frac{1}{a_{max}^4}\right) = \alpha\left(\frac{1}{a^4} - \frac{1}{a_{max}^4}\right) \quad [23]$$

where $\alpha = k'\frac{3\dot{m}^3}{5\pi c}$. Integrating from the initial condition a_o at t_o and writing $a_w^* = a/a_{max}$ for $a > r_b$ gives (see Glover *et al.*, 2016)

$$t - t_o = \frac{1}{4}\frac{a_{max}^5}{\alpha}\left[ln\left(\frac{1+a_w^*}{1-a_w^*}\right) - ln\left(\frac{1+a_o^*}{1-a_o^*}\right) - 4(a_w^* - a_o^*) + 2tan^{-1}a_w^* - 2tan^{-1}a_o^*\right] \quad [24]$$

The group $a_{max}^5/4\alpha$ is a dimensionless timescale, $t_{c,weak}$, which leads to the dimensionless time $t_w^* = t/t_{c,weak}$.

(ii) Strong soil: $a_{max} < r_b$

Glover *et al.* (2016) did not consider the case where a_{max} was small, associated with thick layers, soils with a high yield stress, or relatively low flow rates. Substituting Equation [19] into Equation [2] yields

$$\frac{da}{dt} = k'\frac{3}{5\pi}\dot{m}U_o\left(\frac{1}{a} - \frac{1}{a_{max}}\right) = \sigma\left(\frac{1}{a} - \frac{1}{a_{max}}\right) \quad [25]$$

where $\sigma = k'3\dot{m}U_o/5\pi$. Writing $a_s^+ = a/a_{max}$ for $a < r_b$ yields

$$\frac{da_s^+}{dt_s^+} = \frac{1 - a_s^+}{a_s^+} \quad [26]$$

where t_s^+ is a dimensionless time, *viz*:

$$t_s^+ = \frac{\sigma}{a_{max}^2}t \quad [27]$$

with timescale $t_{c,strong}$.

$$t_{c,strong} = \frac{a_{max}^2}{\sigma} \quad [28]$$

Integrating from the instant where breakthrough is first noticed, a_o^+, at time t_o^+, yields a second implicit relationship

$$t^+ = t_o^+ + \ln\left(\frac{1-a_o^+}{1-a_s^+}\right) + a_o^+ - a_s^+ \qquad [29]$$

which differs noticeably from [24] in its early behaviour (see Supplementary Figure S.1).

Figure 2 shows sets of experimental data obtained for a layers of the petroleum jelly employed in this work. In Figure 2 (a), $a_{max} < r_b$ and the fit to the strong soil model, Eq. [29], is good. Figure 2 (b) shows the agreement with the weak soil model for a case where $a_{max} > r_b$. In both cases the model was fitted to data in the region in which the equations are valid. Both models are able to describe the main features of the experimental data, such as a steep increase in a at the beginning of the cleaning process and the approach to an asymptote. However, they do not provide a reliable description of the growth of the cleaned radius: both models lead to an estimation of a_{max} that is larger than the experimental values. Similar behaviour was also reported by Glover *et al.* (2016) when fitting data to Eq. [24].

The assumption by Glover *et al.* (2016) that the soil-liquid interface, *i.e*. the cleaning front, at a_{max} takes the form of a wedge yields a relationship between a_{max} and $\dot{m}$ which can be compared with experimental data. A force balance in the radial direction over the wedge shown in Figure 3 yields Eq. [3].

Using Eq. [19] to estimate $M = M_y$ at $a = a_{max}$ for the strong soil case yields:

$$a_{max} = \frac{3}{5\pi}\frac{U_o}{\tau_c \delta_o}\ (\sec\chi - 1)\ \dot{m} \qquad [30]$$

while using Eq. [20] for the weak soil case gives

$$a_{max} = \left[\frac{3}{5\pi c}\frac{1}{\tau_c \delta_o}(\tan\chi - \sin\chi)\right]^{0.25} \dot{m}^{0.75} \qquad [31]$$

An explanation for the deviation from the models is obtained by plotting the data in the form of Equation [2], calculating the local cleaning rate by numerical differentiation of $a(t)$ data. M was calculated using the expressions in Table 1. The trend in Figure 4 (a) was observed in all the cleaning experiments reported here: Equation [2] is followed at higher values of M, with the rate proportional to $M - M_y$, where M_y is the intercept on the x-axis. This explains how previous workers were able to describe their results using Equation [2], which is also plotted

in Figure 4 (a). As a increases and M approaches M_y, however, the rate deviates from the linear relationship. Figure 4 (b) shows that the rate approaches zero asymptotically.

M_y is an important parameter. Glover *et al*. linked this quantity to the 'critical stress' of the material by modelling the cleaning front as a ramp of angle χ (Equation [3]) and it will be shown that the shear stress imposed by the liquid film at the surface, τ_w, for cases such as in Figure 4 gives values similar to those where the petroleum jelly exhibits creep in rheological tests. The equations for τ_w proposed by Bhagat and Wilson (2016) are provided in the Supplementary Material, Equations [S.1], [S.2] and [S.3].

The authors are not aware of this transition having been reported previously. A simple quantitative model for the transition is not available and the following semi-empirical expression is proposed:

$$\frac{da}{dt} = k'\left[M - M_y\left(\frac{M}{M + M_y/4}\right)^2\right] \qquad M > M_y/4 \qquad [32a]$$

$$\frac{da}{dt} = 0 \qquad M \leq M_y/4 \qquad [32b]$$

This captures the key features of the transition, namely

(i) A linear dependency of cleaning rate on M at high values of M;

(ii) The rate approaches zero as M approaches zero, and is always positive;

The maximum cleaned radius a_{max} is reached at $M_y/4$ (see the Appendix). Inspection of the data indicated that the value of M calculated at a_{max} was greater than or equal to $M_y/4$ for all the experiments reported here, so Eq. [32a] provides a viable description of the tests. This expression captures a transition in removal mechanisms, which is attributed to a change from displacement of yielded soil, driven by the momentum imposed by the liquid film, to one involving creep. This 'transition model' is found to describe the experimental data well and is compared to previously reported data sets.

For cases where $a_{max} > r_b$ (weak soil), the momentum flow rate of the liquid film can be estimated by Eq. [20] and when $a_{max} < r_b$, M can be described by Eq. [19]. Substituting these results into Eq. [32a] for $a = a_{max}$, and setting $\frac{da}{dt} = 0$ yields:

$$a_{\max} = \frac{12}{5\pi}\frac{U_o \dot{m}}{M_y} \quad [33]$$

for the strong soil, and

$$a_{\max} = \left(\frac{12}{5\pi c}\right)^{1/4}\frac{\dot{m}^{3/4}}{M_y^{1/4}} \quad [34]$$

for the weak soil.

These expressions are compared with the experimental data.

2.3 Traversing nozzle

When a coherent jet with circular cross section impinging normal to the surface traverses across a flat surface it generates a round-nosed band of width w_c clear of soil (see Figure 5). Wilson *et al.* (2015) modelled the shape of the cleaned region where cleaning was described by the weak soil model (Equation [24]), and Bhagat *et al.* (2017) presented results for the strong and intermediate soil cases as well and inclined jets. The model is extended here for viscoplastic soil layers which exhibit an asymptotic limit to cleaning.

Figure 5 shows a jet traversing at velocity v_{jet}, with the impingement point as the frame of reference. Soil is convected towards the jet at velocity v_{jet}, and there is a stationary point at X, distance a_x ahead of the impingement point at O, where $|da/dt|_X = v_{jet}$. At other points, labelled P, at angle β to the path of the jet and distance p from O, vector analysis yields (see Wilson *et al*., 2015)

$$\frac{dp}{d\beta} = \left(\frac{da}{dt}\right)_P \frac{p}{v_{jet}\sin\beta} - \frac{p}{\tan\beta} \quad [35]$$

where $\left(\frac{da}{dt}\right)_P$ is the rate of cleaning at the point P. We consider the case where the cleaning front has been established beyond the nozzle footprint, *i.e.* $a_x > r_o$. Oevermann *et al.* (2019) discussed the case where $a_x < r_o$ and the peeling front only grew in the wake of the nozzle.

Writing $p^* = p/a_x$, i.e. $p^* \geq 1$, yields

$$\frac{dp^*}{d\beta} = \left(\frac{da}{dt}\right)_P \frac{p^*}{v_{jet}\sin\beta} - \frac{p^*}{\tan\beta} \quad [36]$$

Hence the solution depends on the cleaning rate regime. For the weak soil case with $M_y = 0$, $da/dt = \alpha/p^4$. With initial condition $p^* = 1$ at $\beta = 0$ the solution is

$$p^{*4} sin^4\beta = \frac{4}{3}\cos^3\beta - 4\cos\beta + \frac{8}{3} \quad [37]$$

The width of the cleaned region is determined by setting $\beta = \pi$ and gives $w_c = 3.04a_x$. The impact of the different cleaning kinetic expressions for viscoplastic soil layers is now considered.

(i) 'Weak viscoplastic soil'

This is the case considered by Glover *et al*. and requires that $a_x > r_b$. At X

$$\left.\frac{da}{dt}\right|_X = v_{jet} = \alpha\left(\frac{1}{a_x^4} - \frac{1}{a_{max}^4}\right) \quad [38]$$

This offers a check on the model as it predicts that a_x^{-4} increases linearly with v_{jet}. Substituting this result into Equation [36] to eliminate α gives

$$\frac{dp^*}{d\beta} = \underbrace{\frac{1}{p^{*3}\sin\beta} - \frac{p^*}{\tan\beta}}_{\text{Hydrodynamic term}} + \underbrace{\frac{M_{y'}}{p^{*3} v_{jet}\sin\beta}\left(1 - p^{*4}\right)}_{\text{Yield stress term}} \quad [39]$$

where $p^* = p/a_x$ and $M'_y = \alpha/a_{max}^4$. This requires numerical evaluation, with initial condition $p^* = 1$ at $\beta = 0$.

(ii) 'Strong viscoplastic soil'

For Equation [25] to apply, $a_x < r_b$. At X

$$\left.\frac{da}{dt}\right|_X = v_{jet} = \sigma\left(\frac{1}{a_x} - \frac{1}{a_{max}}\right) \quad [40]$$

In this case a_x^{-1} increases linearly with v_{jet}. Elsewhere

$$\left.\frac{da}{dt}\right|_P = \sigma\left(\frac{1}{p} - \frac{1}{a_{max}}\right) \quad [41]$$

and Equation [36] becomes

$$\frac{dp^*}{d\beta} = \underbrace{\frac{1}{\sin\beta} - \frac{p^*}{\tan\beta}}_{\text{Hydrodynamic term}} + \underbrace{\frac{M'_y}{v_{jet}\sin\beta}\left(1 - p^*\right)}_{\text{Yield stress term}} \quad [42]$$

where $M'_y = \sigma/a_{max}$.

Both Equations [39] and [42] feature a hydrodynamic term and a yield stress term. The hydrodynamic terms are similar to the RHS of the moving jet equations proposed by Bhagat *et al.* (2017).

(iii) 'Transition model'

Equation [35] is combined with numerical evaluation of M to calculate the local cleaning rate in the integration of Equation [36]. It is expected to give a better description of the traversing nozzle profiles as the transition model gives a better description of the local cleaning rate for static nozzles. The dependency of a_x on v_{jet} offers a second way of testing the validity of the models. In this case, at point X:

$$\left.\frac{da}{dt}\right|_X = v_{jet} = k' \left[M_X - M_y \left(\frac{M_X}{M_X + M_y/4} \right)^2 \right] \quad [43]$$

where M_X is the momentum flow rate per unit length of the liquid film at a_X.

3. Materials and Methods

3.1. Impinging jet apparatus

The apparatus was described by Glover *et al.* (2016) and consisted of a Perspex® walled 1×1×2 m high cuboidal chamber in which a nozzle directed water on to a vertical target which could be stationary or moved upwards or downwards at a set speed. The targets were made from transparent materials so that cleaning could be monitored by cameras located outside the cabinet. The apparatus was adapted to accommodate detachable 150×150 mm Perspex® and glass target plates. Larger Perspex® plates (360×600 mm) were also used for the moving jet experiments.

De-ionized water was pumped from a 40 L reservoir through a rotameter before entering a 150 mm long pipe of internal diameter 9.5 mm on which a 55° convergent entry brass nozzle with diameter d_N = 2, 3 or 4 mm was mounted. The nozzle was positioned 60 mm from the target to ensure a coherent jet, since longer jets break up due to surface tension effects (Dumouchel, 2008; Feldung Damkjær *et al*., 2017; Chee *et al*., 2019). After the pump was started to initiate flow an interrupter plate was held between the nozzle and target for at least 30 s to ensure a stable jet had formed. The mass flow rates used corresponded to Reynolds numbers in the range 6,500 – 37,000. All tests were conducted at room temperature, approximately 20 °C, and were filmed at 1920×1080 pixels resolution using either (i) 60 frames per second (fps) with a Nikon D3300 D-SLR digital camera, or (ii) 50 fps with a Sony HX80 camera.

A commercial petroleum jelly (GPC5220-5Y, APC Pure, UK) was used as the soil. Petroleum jellies are time-dependent yield stress materials (De Waele, 1949; Park and Song, 2010) and are insoluble in water, so are not subject to soaking effects observed in other layers (e.g. Carbopol, Chee *et al.*, 2018; egg yolk, Yang *et al.*, 2019, Murcek *et al.*, 2019). Layers of uniform thickness δ_0 were prepared using the spreader tool described by Cuckston *et al.* (2019) on the smaller plates, and using the tool described by Glover *et al.* (2016) on the larger plates. The thickness was calculated from the mass applied and the density, measured separately as 812 ±13 kg m^{-3}. The spreading procedure took between 5 and 15 s, so a spreading time of 10 s is taken as indicative of this initial stage.

Images were subsequently processed using a Matlab^{TM} script that detects the shape of the cleaned region by thresholding the intensities of the pixels between the cleaned and uncleaned regions. The radius of the cleaned region was measured at 1˚ intervals, and the effective cleaned radius, a, computed from the average of these 360 measurements. The standard deviation of the measurements of the cleaned radius in each image provides an estimate of the uncertainty of a at each position. Figure 6 (a) shows an example of the crater formed after a jet impinged a 0.86 mm thick layer for $t = 485$ s. Figure 6 (b) shows the image with the detected borders and the circle with effective cleaned radius a. The models are compared to the (a, t) data sets.

3.2. Profilometry of the layers

The shape of the soil layer after exposure to the jet was measured by a confocal thickness sensor (ConfocalDT IFS 2405-3, Micro-Epsilon, Germany) mounted on a computer-controlled *x*-*y* positioning stage. The sample was moved in the horizontal plane with step sizes Δx and Δy, and the local thickness measured to a precision of 36 nm (Micro-Epsilon, 2018). Figure 7 (a) shows the result obtained for the crater generated by a jet with d_N=2 mm, with Δx= Δy=1 mm. The shape of the crater was extracted from linear scans of the profiles, with Δx=0.05 mm. Figure 7 (c) shows the profile of the soil rim at four equally spaced azimuthal angles θ, where l is the distance from the start of the rim, shown schematically in Figure 7 (b). There was a thin residual film of petroleum jelly (thickness of order microns) in the cleared region, indicating that removal did not involve true adhesive detachment from the substrate. Values of two characteristic angles (gradients) were measured, as indicated on Figure 7 (d). These were (*i*) the slope at the base of the rim, labelled ϕ_1, and (*ii*) the gradient of the front at the initial layer height, δ_0, labelled ϕ_2. The Glover *et al*. model assumed a wedge-shaped ramp, *i.e.* $\phi_1 = \phi_2$.

3.3. Rheological characterization

The rheological behaviour of the jelly was studied in a Kinexus Lab+ controlled-stress rheometer (Malvern Instruments, UK), using rough 40 mm diameter parallel plates. Unless stated otherwise, the results were obtained with a 1 mm gap. The temperature was controlled at 20 ºC by a thermostatic bath, matching the ambient temperature of the room in which the jelly was stored and jet tests conducted. After loading the sample using a spatula, the petroleum jelly was pre-sheared at 1 s^{-1} for 10 s to impose a known strain history to the sample.

4. Results and Discussion

4.1 Rheological characterization

Ageing time

Several semi-solid materials, such as petroleum jellies (Park and Song, 2010), exhibit time-dependent behaviour where the critical stress increases over the ageing time as a result of structural recovery (Fernandes *et al*., 2016). According to Mewis and Wagner (2009), a non-destructive way to quantify the structural recovery is to apply a low amplitude oscillatory shear at constant strain or stress amplitude. If the material is probed in the linear viscoelastic regime, the microstructural recovery of the material is quantified by the evolution of the storage modulus, G', over time.

Figure 8 (a) presents the elastic modulus, G', and the loss modulus, G'', for the petroleum jelly obtained with a stress amplitude of 1 Pa and frequency 1 Hz over 1800 s. The former reaches a limiting value of approximately 70 kPa after 600 s. Moreover, G' is considerably larger than G'', indicating viscoelastic (semi-solid) behaviour of the material when at rest (Ewoldt *et al.*, 2010; Ewoldt and McKinley, 2017). On the basis of these data an ageing (wait) time of 30 min was observed after coating to ensure that the soil was in a reproducible state at the start of each cleaning experiment. Figure 8 (b) shows the shear stress amplitude imposed in the oscillatory test, and the resultant shear strain amplitude as a function of time. The latter is around 0.002%, confirming that the response is in the linear viscoelastic regime (Hyun *et al*., 2011; Macosko, 1994).

Creep tests

Coussot *et al.* (2002) described the use of creep testing to evaluate the critical stress of thixotropic yield stress materials. A constant shear stress is imposed and the resultant shear rate allows an instantaneous viscosity to be calculated. A bifurcation in viscosity evolution is observed at the critical stress. The method is strongly dependent on the time scale of the test, since delayed yielding can occur below the values associated with the critical stress probed at shorter time-scales (Bonn *et al.*, 2015). A characteristic time-scale representative of the application must therefore be chosen to estimate the critical stress. The time-scale of the cleaning experiments ranged from 0.2 to 600 s.

Figure 9 (a) presents the shear rate as a function of time for creep tests lasting 300 s, for a series of different imposed shear stresses. There is a noticeable change in behaviour between 212 Pa and 214 Pa, exhibiting the transition reported by Coussot *et al*. Below 212 Pa, the material creeps and the shear rate tends to low values, indicating a predominantly elastic regime. Shear stresses above 214 Pa lead to higher values of shear rate, indicating a viscous response (Da Cruz *et al*., 2002). This gives a critical stress, τ_c, for this material of 212 Pa.

The critical stress can also be determined using increasing steady shear stress ramps starting from rest (Chang *et al.*, 1998). The shear stress was increased at $\dot{\tau}$ = 10 Pa/min, using rough parallel plates. Some experiments were also performed with a (relatively smooth) Perspex base to check if wall slip is likely to arise with surfaces similar to those used in the cleaning experiments. Dimitriou *et al.* (2011) observed wall slip in model waxy crude oils on smooth surfaces: these partially crystallised materials are similar in nature to the petroleum jelly. Different gaps were used, following the Yoshimura and Prud`homme (1988) protocol for studying wall slip. Figure 9 (b) compares results obtained with the rough base (gap 1.0 mm), and with the smooth Perspex base with 0.5 and 1.0 mm gaps. At strains above 0.1%, the material response is roughly independent of both surface and gap, indicating that wall slip is unlikely to take place in the cleaning experiments. However, slip effects were evident at strains below 0.1%, which were enhanced by a (i) smoother surface and (ii) smaller gap. The plot shows the intersection between two power-law curves, one fitted below and one above the transition from the elastic response to the viscous regime, giving $\tau_c \cong 220$ Pa, which is in agreement with the value obtained from creep testing. Above the critical stress, the data could be fitted by the Herschel-Bulkley model, with parameters $\tau_{c,HB}$ = 275 Pa, k_{HB}=23.6 Pa.s$^{0.44}$

and n_{HB}=0.44. The critical stress found by fitting the Herschel-Bulkley equation to the data above the transition point is larger than the value obtained from creep testing. This is a result of the material being probed in a transient experiment.

4.2 Cleaning Experiments

The evolution of the cleaning front is presented in Figure 10 for three repetitions at the same experimental condition, using Perspex and glass plates, with the average value of a plotted against the time elapsed since breakthrough was first seen. The larger error bars at longer times arise from asymmetry in the cleared region. This is evident in the circularity data which are presented in Supplementary Figure S.2. The effect of the substrate is smaller than the difference between repeats. Therefore, Perspex substrates were used for the remaining experiments reported. In all cases the cleaning front reaches a limit, a_{max}, which in the majority of the cases is larger than r_b. One of the cases in which a_{max} lay within the boundary layer formation zone is reported in Figure 2(a). The cleaning region is initially circular: at r_t, fingering starts to take place and the cleaning region departs from a circular shape. Supplementary Figure S.2 presents the analysis of the circularity of one of the experiments reported in Figure 10.

Figure 11 (a) shows the data from different cleaning experiments presented in the form of Eq. [2], where M was calculated using Equation [18]. When the momentum flow rate imposed by the liquid film is high, the evolution of da/dt with M is approximately linear, indicating that a simple rate law such as Eq. [2] is sufficient to describe the evolution of the cleaned radius over time at the early stages of cleaning. Non-linear behaviour is observed at large a as da/dt approaches zero, which is not captured by the simple adhesion model. Also shown are the fits of Eq. [32a] to the datasets, indicating that the transition model is able to describe the variation in da/dt for experiments with different ranges of M. Integration of Eq. [32a] leads to the estimate of a over t shown in Figure 11 (b). Both the rapid initial growth and the asymptotic behaviour are described well by the transition model. In some cases the model deviates from the experimental data when $a > r_b$, as shown for the case with $d_N = 4$ mm, $Q = 5$ L/min and $\delta_o = 0.50$ mm. This behaviour was also reported by Feldung Damkjær *et al.* (2017), and the reason for this is not currently understood.

Figure 11(c) shows the cleaning rate plotted against the shear stress imposed by the liquid film on the soil surface, τ_w, for the experimental conditions in Figure 11(a) and (b). The

shear stress imposed by the liquid film is lower than τ_c obtained from the rheometry tests. This suggests that the jelly is creeping under the force imposed by the liquid film, leading to the non-linear relationship between da/dt and M reported in Figure 11(a). This non-linear behaviour is captured by the transition model.

4.3 Crater topography

The shape of the rims of the cleaned area was determined with the confocal profilometer. The angles ϕ_1 and ϕ_2 are reported in Figure 12(a) as a function of the ratio between the thickness of the liquid film h, calculated using Eq. [7], [10] or [13], and the thickness of the undisturbed soil layer, δ_o. The asymptotic cases, in which the soil layers were exposed to the impinging jet until a approached a_{max}, as well as interrupted experiments are reported.

Two distinct regimes are evident: when $h/\delta_o \leq 0.4$, ϕ_1 and ϕ_2 differ, indicating that the rim shape is not a simple wedge as assumed by Glover *et al.* (2016). For $h/\delta_o > 0.4$, however, the values of ϕ_2 gradually approach those of ϕ_1. The values of ϕ_2 for $\frac{h}{\delta_o} \leq 0.4$ are close to 45°, whereas with thicker liquid films the slope is more gradual, rising from 10° to 30°. An angle of 45° suggests that the radial momentum flow rate of the thin film generates internal yield of the soil layer.

The thickness of the liquid film generated by an impinging jet changes with the radial position (Bhagat and Wilson, 2016), and so the value of h/δ_o changes over a cleaning experiment. A plate coated with a δ_o=0.37 mm layer was exposed to an impinging jet with Q =2 L/min for different lengths of time and the rim shape measured. The values of ϕ_1 and ϕ_2 obtained are presented in Figure 12 (b). The same trend is evident, indicating that h/δ_o is the governing factor determining the shape of the rims throughout the cleaning process.

4.4 Cleaning by moving jets

Moving jet experiments were performed with petroleum jelly layers of thickness ranging from 0.194 to 1.05 mm on vertical Perspex plates. Constant water flow rates were used, with $1 \leq Q \leq 2$ L/min and a 2 mm nozzle. The transverse velocity of the target plates ranged from 8.9 to 155 mm/s. As discussed by Glover *et al.* (2016), the cleaning front generated by a

moving jet impinging on the moving substrate is more stable when the plate moved downwards rather than upwards, due to the jet impinging on an undisturbed layer. Therefore, all the experiments reported here were conducted with the plate moving downwards.

Figure 13 (a) presents the shape of the cleaned region generated by a moving jet ($Q = 2$ L/min; $\delta_o = 0.33$ mm; $v_{jet} = 15.09$ mm/s), along with the estimates of the cleaned region provided by the different cleaning models. The value of k' used for each case was found by fitting the corresponding model to the a vs t data obtained using a static nozzle. Both the strong and the transition soil formulations provide good descriptions of the shape of the cleaned region near the point of impingement, where the cleaned radius is small and da/dt is high. The biggest difference between these two models occurs beyond r_b^* where da/dt is small and the strong soil model fails to describe the non-linear relationship between da/dt and M (see Figure 4). The transition model, on the other hand, describes the shape of the cleaned region from the initial stages up to a_{max}^*. Beyond a_{max}^* there is no change and the cleaning front is a horizontal line with width w_c.

The weak viscoplastic soil model did not give a good description of the shape of the cleaned region. This is because this model is fitted for $a > r_b$, where da/dt is lower than in the boundary layer formation region. The value of k' obtained with the weak soil model is thus smaller than the value of k' obtained with the strong soil and with the transition model, resulting in $\left(\frac{da}{dt}\right)_P$ in Eq. [35] being underestimated and limiting the value of w_c obtained.

This is demonstrated in Figure 13 (b), where the value of k' found by fitting the weak and strong viscoplastic soil models are compared with k' found by fitting the transition model to the asymptotic cases. k' estimated with both the weak and strong viscoplastic soils is smaller than k' found by fitting the transition model. Additionally, the values of k' for the strong viscoplastic soil model are larger than those obtained with the weak version. Care therefore needs to be taken in comparing absolute values of k' obtained using different models.

Equations [38], [40] and [43] describe the relationship between a_X and v_{jet} expected for the three models. Figure 14 (a)-(d) presents the values of a_x as a function of v_{jet} for moving jet experiments conducted with different soil layer thicknesses and flow rates. The transition model gives the most reliable description of the dependence of a_x on v_{jet}. The strong viscoplastic soil model gives reasonable agreement in two cases. The values of a_x all lie below

r_b for each set of conditions and the weak viscoplastic soil model does not therefore describe the data well. A plot of w_c as a function of v_{jet} is presented in Supplementary Figure S.3.

Figure 15 (a) shows the observed values of w_c plotted against a_x for all the moving jet experiments conducted, with different values of Q, v_{jet} and δ_o. Fitting the data to a linear trend gave w_c/a_x=3.04, which is similar to the result reported by Bhagat *et al.* (2017) using the adhesive failure weak soil. It should be noted that the latter model would not predict a_x correctly (as $a_x < r_b$ in most cases) so this would appear to be a fortuitous coincidence. Eq. [35] was solved numerically, using the transition model, to estimate the rate of cleaning at each point on the front, giving w_c. The results in Figure 15 (b) follow the relationship w_c/a_x= 3, with noticeable scatter at larger a_x, which represents good agreement with the experimental trend.

4.5 Parameter analysis – static nozzles

The transition model was fitted to the experimental data reported in this study and those reported by Feldung Damkjær *et al.* (2017) and Glover *et al.* (2016) using different petroleum jellies. The parameters k' and M_y are compared in Figure 16 (a). There is no clear relationship between k' and M_y for each data set, and there is a noticeable difference between the values of k' for each petroleum jelly. Figure 16 (b) presents the values of a_{max} and M_y in the form suggested by Eq. [34] for cases where $a_{max} > r_b$, *i.e.* in the weak soil region. The inset presents the data in the form proposed by Eq. [33] for the strong soil cases. Both show linear trends, indicating that the wedge model captures some elements of the mechanism.

Figure 16 (c) and (d) compare the performance of the transition model with the model of Glover *et al.* (2016). Figure 16 (c) shows that the latter give estimates which agree with the experimental values within error bands of ±50 % whereas the transition model gives agreement within ±15 %. This indicates that the transition model is able to describe the evolution of the cleaned radius for a viscoplastic soil layer more reliably than the earlier model, principally because it includes a term to account for the creep seen in the rheological tests. Good agreement was also found in linking the results from static and moving nozzles.

Figure 17 compares the measurements of the shape of the cleaning front at a_{max}, ϕ_1 and ϕ_2 in Figure 12(a), with that calculated using the wedge assumption (Eq. [3]). These calculations employed the value of the critical stress identified in Section 4.1 for τ_c. The values of χ are comparable to the values of ϕ_2, indicating that the deformation occurring at the rim

includes a significant contribution from shear of the viscoplastic fluid. More detailed modelling is required to predict the shape of the rim, and the reason for the change in angle at $h/\delta_0 \sim 0.4$. Glover *et al*. (2016) reported χ values in the range 10-25° using the weak soil model to estimate M_y. This tends to overestimate M at smaller a, where asymptotic behaviour is observed (see Figure 1), which may explain the difference from the values obtained here.

The transition model is not a predictive tool in that the parameters k' and M_y are obtained by fitting of experimental data. The measurements of the shape of the cleaning front indicate that the simple wedge-shaped model of Glover *et al.* (2016) does not give a full description of the cleaning mechanism, and further work is required to link the rheology (including creep) of the soil to the liquid layer hydrodynamics.

A second topic requiring further work is the effect of jet break-up, observed with longer jets and other flow rates likely to be employed in industrial cleaning-in-place systems. The impact of jet break-up on the size of the radial flow zone and cleaning behaviour has been investigated by Feldung Damkjaer *et al*. (2017) and Chee *et al.* (2019). The latter study included a careful investigation of the transition from a coherent jet to a disrupted one: the difference in cleaning performance could not be accounted for simply in terms of the amount of liquid lost from the thin film due to splatter.

5. Conclusions

The models for cleaning soil layers from flat surfaces by coherent impinging liquid jets proposed by Wilson *et al.*(2015, 2014), Bhagat *et al.* (2017) and Glover *et al.* (2016) have been revisited, in order to establish whether they can be used to describe cleaning of a hydrophobic viscoplastic soil layer. The radial rate of cleaning was evaluated in terms of the momentum flow rate imposed by the liquid film, using the Bhagat and Wilson (2017) hydrodynamic description for the flow in the thin film generated by an impinging liquid jet. The strong soil and the weak soil models proposed by Bhagat *et al.* (2017) were adapted in order to account for a yield term. Our results indicate that the adhesive failure model proposed by Glover *et al.*, which proposes a linear relationship between da/dt and $M - M_y$, is not valid as $M \to M_y$ due to the nature of the petroleum jelly used, which exhibits creep at shear stresses approaching the critical stress. A transition model is proposed and which describes the evolution of the cleaned radius over time. The non-linear rate dependency observed is attributed to a creeping flow

mode at the later stages of cleaning. The model was able to accurately describe the evolution of the radius of the cleaned area and the relationship between the model parameters follows the expected trends.

The models were adapted to describe cleaning of the soil by a moving nozzle: the strong viscoplastic soil and the transition models both provided appropriate descriptions of the shape of the trail generated by the moving nozzle.

OPEN DATA

A statement providing a link to the data reported in this paper on the University of Cambridge Apollo data repository will be included here if the manuscript is accepted for publication

ACKNOWLEDGEMENTS

This study was financed in part by the Coordenação de Aperfeiçoamento de Pessoal de Nível Superior - Brasil (CAPES) - Finance Code 001, by the provision of a PhD studentship for RRF. ERASMUS funding for DO from the European Union, as well as helpful discussions with Rajesh Bhagat and Melissa Chee, are also gratefully acknowledged.

References

Barnes, H.A., 1999. The yield stress—a review or ‘παντα ρει’—everything flows? J. Non-Newtonian Fluid Mech 81, 133–178. https://doi.org/10.1016/S0377-0257(98)00094-9

Bhagat, R.K., Jha, N.K., Linden, P.F., Wilson, D.I., 2018. On the origin of the circular hydraulic jump in a thin liquid film. J. Fluid Mech. 851, R5. https://doi.org/10.1017/jfm.2018.558

Bhagat, R.K., Perera, A.M., Wilson, D.I., 2017. Cleaning vessel walls by moving water jets: Simple models and supporting experiments. Food Bioprod. Process. 102, 31–54. https://doi.org/10.1016/j.fbp.2016.11.011

Bhagat, R.K., Wilson, D.I., 2016. Flow in the thin film created by a coherent turbulent water jet impinging on a vertical wall. Chem. Eng. Sci. 152, 606–623. https://doi.org/10.1016/j.ces.2016.06.011

Bonn, D., Denn, M.M., Berthier, L., Divoux, T., Manneville, S., 2015. Yield Stress Materials in Soft Condensed Matter. arXiv 1502.05281, [cond-soft]. https://doi.org/10.1103/RevModPhys.89.035005

Chang, C., Boger, D. V, Nguyen, Q.D., 1998. The Yielding of Waxy Crude Oils. Ind. Eng. Chem. Res. 5885, 1551–1559.

Chee, M.W.L., Ahuja, T.V., Bhagat, R.K., Taesopapong, N., Wan, S.A., Wigmore, R.L., Wilson, D.I., 2018. Impinging jet cleaning of tank walls: effect of jet length, wall curvature and related phenomena. Food Bioprod. Process. 1–12. https://doi.org/10.1016/j.fbp.2018.10.005

Coussot, P., Nguyen, Q.D., Huynh, H.T., Bonn, D., 2002. Viscosity bifurcation in thixotropic, yielding fluids. J. Rheol. 46, 573–589. https://doi.org/10.1122/1.1459447

Cuckston, G.L., Alam, Z., Goodwin, J., Ward, G., Wilson, D.I., 2019. Quantifying the e ff ect of solution formulation on the removal of soft solid food deposits from stainless steel substrates. J. Food Eng. 243, 22–32. https://doi.org/10.1016/j.jfoodeng.2018.08.018

Da Cruz, F., Chevoir, F., Bonn, D., Coussot, P., 2002. Viscosity bifurcation in granular materials, foams, and emulsions. Phys. Rev. E 66, 051305. https://doi.org/10.1103/PhysRevE.66.051305

Dimitriou, C.J., McKinley, G.H., Venkatesan, R., 2011. Rheo-PIV Analysis of the Yielding and Flow of Model Waxy Crude Oils. Energy & Fuels 25, 3040–3052. https://doi.org/10.1021/ef2002348

Dinkgreve, M., Fazilati, M., Denn, M.M., Bonn, D., Dinkgreve, M., Fazilati, M., Denn, M.M., Bonn, D., 2018. Carbopol : From a simple to a thixotropic yield stress fluid. J. Rheol. 62, 773–780. https://doi.org/10.1122/1.5016034

Dumouchel, C., 2008. On the experimental investigation on primary atomization of liquid streams. Exp. Fluids 45, 371–422. https://doi.org/10.1007/s00348-008-0526-0

Ewoldt, R.H., McKinley, G.H., 2017. Mapping thixo-elasto-visco-plastic behavior. Rheol. Acta. https://doi.org/10.1007/s00397-017-1001-8

Ewoldt, R.H., Winter, P., Maxey, J., McKinley, G.H., 2010. Large amplitude oscillatory shear of pseudoplastic and elastoviscoplastic materials. Rheol. Acta 49, 191–212. https://doi.org/10.1007/s00397-009-0403-7

Feldung Damkjær, N., Adler-Nissen, J., Jensen, B.B.B., Wilson, D.I., 2017. Flow pattern and cleaning performance of a stationary liquid jet operating at conditions relevant for industrial tank cleaning. Food Bioprod. Process. 101, 145–156. https://doi.org/10.1016/j.fbp.2016.11.001

Fernandes, R.R., Andrade, D.E.V., Franco, A.T., Negrão, C.O.R., 2016. Correlation between the gel–liquid transition stress and the storage modulus of an oil-based drilling fluid. J. Nonnewton. Fluid Mech. 231, 6–10. https://doi.org/10.1016/j.jnnfm.2016.02.003

Fryer, P.J., Asteriadou, K., 2009. A prototype cleaning map: A classification of industrial cleaning processes. Trends Food Sci. Technol. 20, 255–262. https://doi.org/10.1016/j.tifs.2009.03.005

Glover, H.W., Brass, T., Bhagat, R.K., Davidson, J.F., Pratt, L., Wilson, D.I., 2016. Cleaning of complex soil layers on vertical walls by fixed and moving impinging liquid jets. J. Food Eng. 178, 95–109. https://doi.org/10.1016/j.jfoodeng.2015.12.021

Hyun, K., Wilhelm, M., Klein, C.O., Cho, K.S., Nam, J.G., Ahn, K.H., Lee, S.J., Ewoldt, R.H., McKinley, G.H., 2011. A review of nonlinear oscillatory shear tests: Analysis and application of large amplitude oscillatory shear (LAOS). Prog. Polym. Sci. 36, 1697–1753. https://doi.org/10.1016/j.progpolymsci.2011.02.002

Kaye, P.L., Pickles, C.S.J., Field, J.E., Julian, K.S., 1995. Investigation of erosion processes as cleaning mechanisms in the removal of thin deposited soils. Wear 186–187, 413–420. https://doi.org/10.1016/0043-1648(95)07152-0

Köhler, H., Stoye, H., Mauermann, M., Weyrauch, T., Majschak, J.-P., 2015. How to assess cleaning? Evaluating the cleaning performance of moving impinging jets. Food Bioprod. Process. 93, 327–332. https://doi.org/10.1016/j.fbp.2014.09.010

Macosko, C.W., 1994. Rheology: principles, measurements, and applications. Wiley - VCH, New York.

Mewis, J., Wagner, N.J., 2009. Thixotropy. Adv. Colloid Interface Sci. 147–148, 214–227. https://doi.org/10.1016/j.cis.2008.09.005

Mickaily, E.S. and Middleman, S, 1993, Hydrodynamic cleaning of a viscous film from the inside of a long tube, *AIChEJ,* 39(5):885 – 893.

Micro-Epsilon, 2018. ConfocalDT Catalog. Ortenburg.

Murcek, R., Schöhl, E., Köhler, H., Boye, A., Gold, S., 2019. Development of a method to determine normal and shear stress necessary to remove a swollen soil from a surface. Food Bioprod. Proc. 113, 86–92. https://doi.org/10.1016/j.fbp.2018.11.009

Oevermann, D., Bhagat, R.K., Fernandes, R.R., Wilson, D.I., 2019. Quantitative modelling of the erosive removal of a thin soil deposit by impinging liquid jets. Wear 422–423, 27–34. https://doi.org/10.1016/j.wear.2018.12.056

Park, E.-K., Song, K.-W., 2010. Rheological evaluation of petroleum jelly as a base material in ointment and cream formulations with respect to rubbing onto the human body. Korea Aust. Rheol. J. 22, 279–289.

Rodgers, A., de Boer, G., Murray, B., Scott, G., Kapur, N., 2019. An investigation in to batch cleaning using wash racks. Food Bioprod. Process. 113, 118–128. https://doi.org/10.1016/j.fbp.2018.11.003

Hsu, T.T., Walker, T.W. Frank, C.W., Fuller, G.G., 2011, Role of fluid elasticity on the dynamics of rinsing flow by an impinging jet. Phys. Fluids. 23, 03310.

Walker, T.W., Hsu, T.T., Frank, C.W. Fuller, G.G. 2012, Role of shear-thinning on the dynamics of rinsing flow by an impinging jet. Phys. Fluids. 24, 093102.

Watson, E.J., 1964. The radial spread of a liquid jet over a horizontal plane. J. Fluid Mech. 20, 481. https://doi.org/10.1017/S0022112064001367

Wilson, D.I., Atkinson, P., Köhler, H., Mauermann, M., Stoye, H., Suddaby, K., Wang, T., Davidson, J.F., Majschak, J., 2014. Cleaning of soft-solid soil layers on vertical and horizontal surfaces by stationary coherent impinging liquid jets. Chem. Eng. Sci. 109, 183–196. https://doi.org/10.1016/j.ces.2014.01.034

Wilson, D.I., Köhler, H., Cai, L., Majschak, J.-P., Davidson, J.F., 2015. Cleaning of a model food soil from horizontal plates by a moving vertical water jet. Chem. Eng. Sci. 123, 450–459. https://doi.org/10.1016/j.ces.2014.11.006

Wilson, D.I., Le, B.L., Dao, H.D.A., Lai, K.Y., Morison, K.R., Davidson, J.F., 2012. Surface flow and drainage films created by horizontal impinging liquid jets. Chem. Eng. Sci. 68, 449–460. https://doi.org/10.1016/j.ces.2011.10.003

Yang, J., Kjellberg, K., Jensen, B.B.B., Nordkvist, M., Gernaey, K. V., Krühne, U., 2019. Investigation of the cleaning of egg yolk deposits from tank surfaces using continuous and pulsed flows. Food Bioprod. Process. 113, 154–167. https://doi.org/10.1016/j.fbp.2018.10.007

Yeckel, A., Middleman, S., 1987. Removal of a viscous film from a rigid plane surface by an impinging liquid jet. Chem. Eng. Commun. 50, 165–175. https://doi.org/10.1080/00986448708911823

Yoshimura, A., Prud'homme, R.K., 1988. Wall Slip Corrections for Couette and Parallel Disk Viscometers. J. Rheol. 32, 53–67. https://doi.org/10.1122/1.549963

Nomenclature

Roman symbols

a	[m]	Radius of the circular cleaned region
A	[-]	Parameter of Eq. [21]
a_{o}	[m]	Initial cleaned radius for Eq. [24]
a_{o}^{+}	[m]	Cleaned radius in which breakthrough is first noticed, Eq. [29]
$a_{\max}$	[m]	Maximum cleaned radius
a_{o}	[m]	First observed cleaned radius
a_{s}^{+}	[m]	Dimensionless cleaned radius, strong soil – Eq. [26]
a_{w}^{*}	[-]	Dimensionless cleaned radius, weak soil – Eq. [24]
B	[m^{-3}]	Parameter of Eq. [21]
c	[$kg^2 \cdot m^{-4} \cdot s^{-1}$]	Group of liquid properties: $c = 10\pi^2\rho\mu/3$
d_N	[m]	Diameter of the nozzle
E	[-]	Edge of the rim
h	[m]	Liquid film thickness
k'	[$m \cdot s \cdot kg^{-1}$]	Cleaning rate constant
k_{HB}	[Pa. $s^{n_{HB}}$]	Consistency index from Herschel-Bulkley equation
l	[m]	Distance from the beginning of the rim
M	[N m^{-1}]	Momentum flow rate per unit length
M_{X}	[N m^{-1}]	Momentum flow rate of the liquid film at a_{X}
M_{y}	[N m^{-1}]	Momentum flow rate required to yield the soil layer
n_{HB}	[-]	Exponent from Herschel-Bulkley equation
O	[-]	Point of impingement
P	[-]	Point of reference for the cleaning front, moving jet
p	[m]	Radial distance to cleaning front, Figure 13
p^{*}	[-]	Dimensionless radial distance to cleaning front
r_{b}	[m]	Radial position where the boundary layer reaches the free surface
r_{o}	[m]	Radius of the nozzle
Re_{j}	[-]	Reynolds number in the jet: $Re_{jet} = \rho U_o d_N/\mu$
r_{j}	[m]	Radial location of the hydraulic jump
t	[s]	Time
t_{o}	[s]	Initial time for Eq. [24]
t_{o}^{+}	[m]	Time in which breakthrough is first noticed, Eq. [29]
$t_{\mathrm{c,strong}}$	[-]	Dimensionless timescale for the strong viscoplastic soil model, Eq. [28]
$t_{\mathrm{c,weak}}$	[-]	Dimensionless timescale for the weak viscoplastic soil model, Eq. [24]
t_{s}^{+}	[-]	Dimensionless time, strong soil – Eq. [27]
t_{o}	[s]	Time when the first cleaned radius is observed
t_{w}^{*}	[-]	Dimensionless time, weak soil – Eq. [24]
U	[m s^{-1}]	Average velocity in the liquid film
U_{o}	[m s^{-1}]	Average velocity in the jet
v_{jet}	[m s^{-1}]	Nozzle traverse speed
w_{c}	[m]	Width of cleared region
z	[-]	Co-ordinate normal to the substrate

715 Greek symbols

α	[$m^5 \cdot s^{-1}$]	Lumped parameter in Eq. [23]
β	[°]	Angle to direction of nozzle motion
χ	[˚]	Angle of inclination of the wedge to the substrate surface
δ_0	[m]	Thickness of the undisturbed soil layer
δ	[m]	Thickness of the soil layer
γ	[-]	Shear strain
$\dot{\gamma}$	[s^{-1}]	Shear rate
ϕ_1	[˚]	Slope measured at the base of the rim
ϕ_2	[˚]	Slope measured at the initial layer height
μ	[Pa.s]	Dynamic viscosity of the liquid
θ	[˚]	Azimuthal angle
ρ	[kg/m^3]	Density of the liquid
σ	[$m^2 \cdot s^{-1}$]	Lumped parameter in Eq. [25]
σ_a	[m]	Standard deviation of the measurements of the cleaned radius
$\dot{\tau}$	[Pa/min]	Rate of increase of shear stress in rheology experiments
τ_c	[Pa]	Critical shear stress of the material
$\tau_{c,HB}$	[Pa]	Critical stress from Herschel-Bulkley equation
τ_w	[Pa]	Wall shear stress

Acronyms

CIP	Cleaning-in-place
FMCG	Fast-moving consumer goods
fps	Frames per second
RHS	Right hand side

720

Table 1 – Bhagat and Wilson (2016) model results for mean velocity, film thickness and momentum flux in the radial thin film.

		Quantity					
	Region	U		h		M	
Bhagat and Wilson (2016)	Boundary layer formation zone $r_o < r < r_b$	$U = \frac{U_o}{8\frac{r}{d_N}\left[0.125\left(\frac{d_N}{r}\right) + \frac{1.06}{\sqrt{Re_j}}\left(\frac{r}{d_N}\right)^{1/2}\right]}$	[6]	$h = d_N\left[0.125\left(\frac{d_N}{r}\right) + \frac{1.06}{\sqrt{Re_j}}\left(\frac{r}{d_N}\right)^{\frac{1}{2}}\right]$	[7]	$M = -0.163198\rho^{0.5}U_o^{1.5}\sqrt{\mu r} + \rho U_o^2 d_N\left[0.125\left(\frac{d}{r}\right) + \frac{1.06}{\sqrt{Re_j}}\left(\frac{r}{d}\right)^{0.5}\right]$	[8]
	Laminar film zone $r_b < r < r_t$	$U = \frac{U_0}{8\frac{r}{d_N}\left[\frac{3.792}{Re_j}\left(\frac{r}{d_N}\right)^2 + 0.1975\left(\frac{d_N}{r}\right)\right]}$	[9]	$h = d_N\left[\frac{3.792}{Re_j}\left(\frac{r}{d_N}\right)^2 + 0.1975\left(\frac{d_N}{r}\right)\right]$	[10]	$M = \frac{0.9302\rho U_o^2 d_N^3}{16r^2\left[\frac{3.792}{Re_j}\left(\frac{r}{d_N}\right)^2 + 0.1975\left(\frac{d_N}{r}\right)\right]}$	[11]
	Turbulent region $r > r_t$	$U = \frac{U_0}{\frac{0.167}{Re_j^{0.25}}\left(\frac{r}{d_N}\right)^{9/4} + 2.37 - 0.0108Re_j^{1/2}}$	[12]	$h = d_N\left[\frac{0.0209}{Re_j^{1/4}\left(\frac{r}{d}\right)^{5/4}} + \left(0.296 - 0.001356Re_j^{1/2}\right)\left(\frac{d_N}{r}\right)\right]$	[13]	$M = \frac{\rho\frac{64}{63}\frac{Q}{2\pi}U_o}{r\left[\frac{0.167}{Re_j^{0.25}}\left(\frac{r}{d_N}\right)^{9/4} + \left(2.37 - 0.0108Re_j^{1/2}\right)\right]}$	[14]
Wilson *et al.* (2012)		$\frac{1}{U} - \frac{1}{U_o} = \frac{10\mu}{3\rho r_o^4 U_o^2}(r^3 - r_o^3)$	[15]	$h = \frac{Q}{2\pi r U}$	[16]	$M = \frac{6}{5}\rho U^2 h$	[17]

Figures

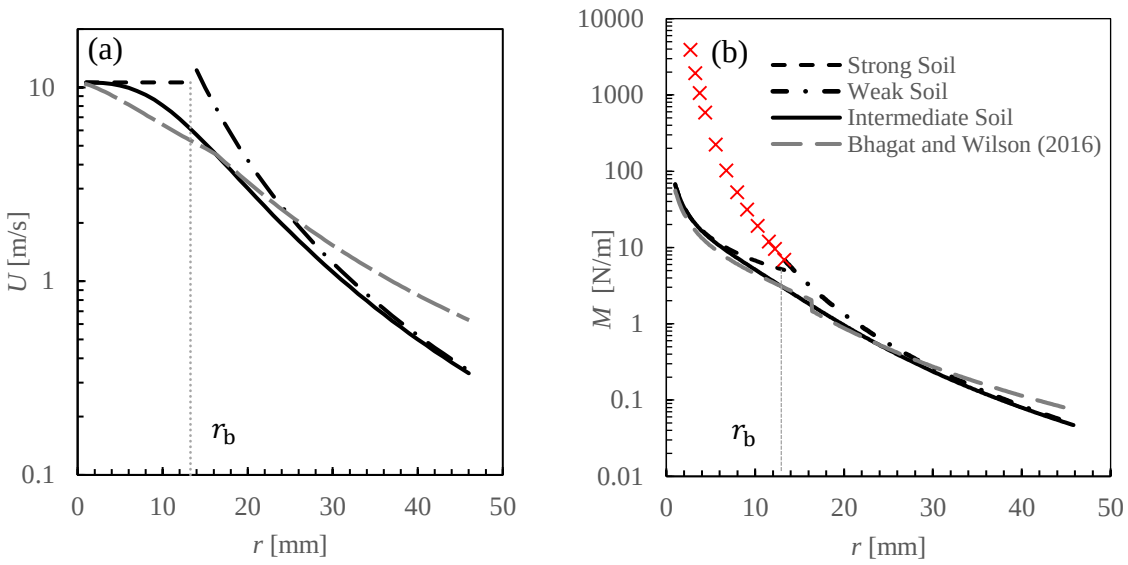

Figure 1 – Comparison between (a) average velocity in the liquid film, and (b) momentum flow rate, as a function of the radial position, r, for the different hydrodynamic models for a water jet at 20 °C, $d_N = 2$ mm and Q = 2.0 L min^{-1}. Lines denote the estimates provided with the strong soil, weak soil, intermediate soil and Bhagat and Wilson (2016) models. Crosses indicate the estimate of momentum flow rate given by the weak soil model below r_b.

735

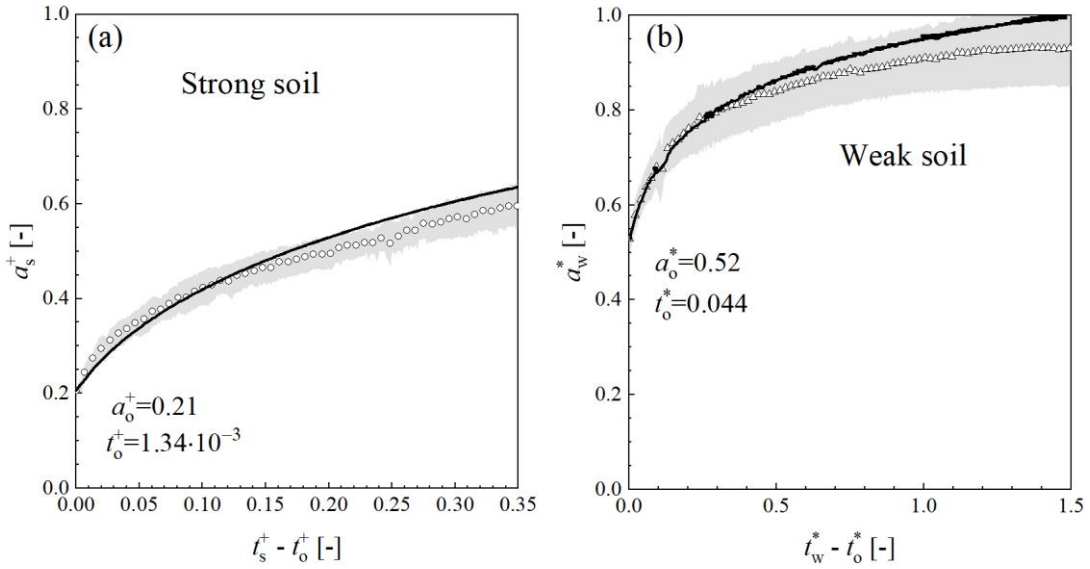

Figure 2. Agreement of analytical models with experimental data. (*a*) strong soil, $a_{\max} < r_b$, Equation [29]: Q =3 L/min, $d_N = 4$ mm, δ_o=1.05 mm. $k' = 4.5 \times 10^{-4}$ m · s · kg^{-1}; (*b*) weak soil, $a_{\max} > r_b$, Equation [24]: Q =2 L/min, $d_N = 2$ mm, δ_o=0.85 mm; $k' =$ 7×10^{-4} m · s · kg^{-1}. Symbols – experimental data; lines – model. Shaded area represents the normalized standard deviation of the measured radii, (standard deviation)/$a_{\max}$, with a maximum value of 11%.

740

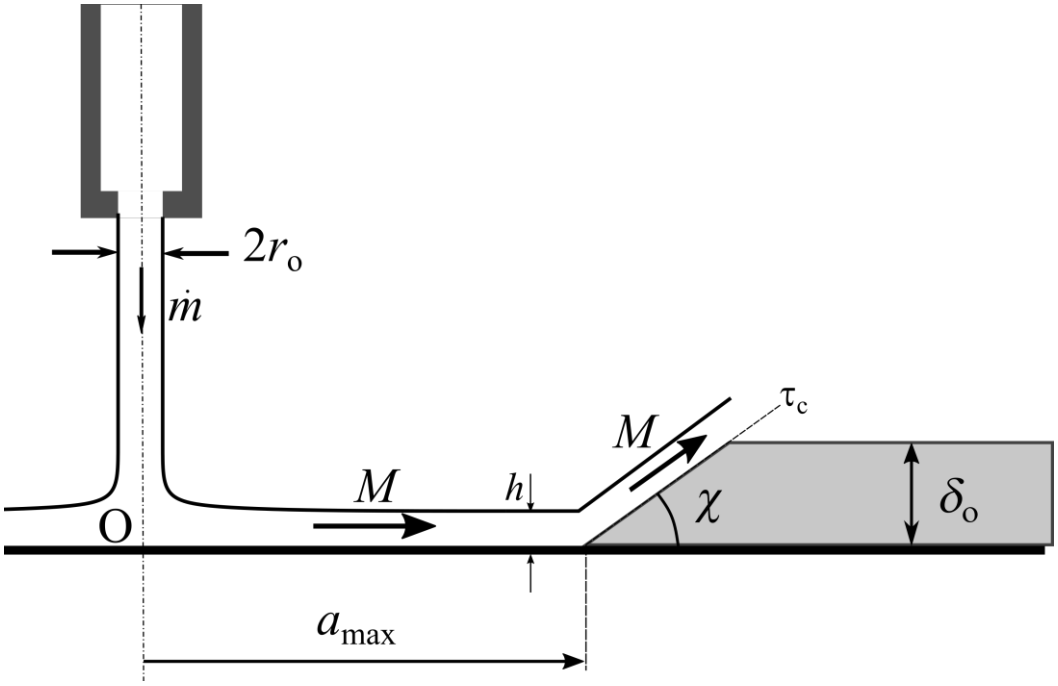

745 Figure 3 – Schematic of the flow at the maximum cleaned radius as proposed by Glover *et al.* (2016)

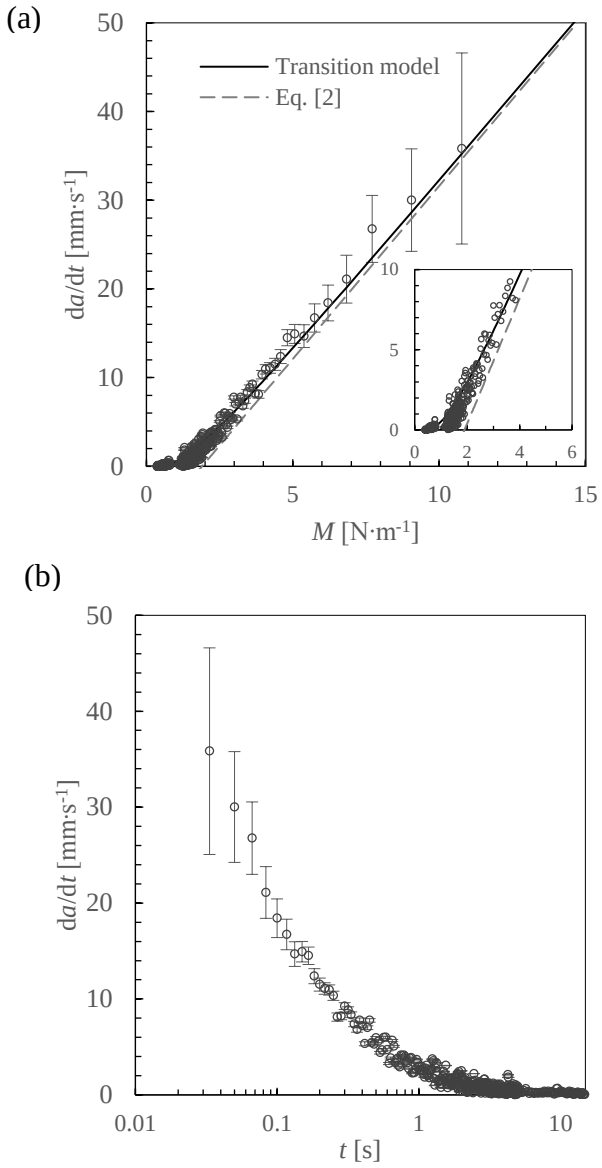

750 Figure 4 – Example of the evolution of the cleaned radius. Conditions: $d_N = 2$ mm; $Q = 1.4$ L/min; δ_o =0.37 mm. (a) da/dt vs M; (b) da/dt vs t. Error bars represent the propagated uncertainty in da/dt.

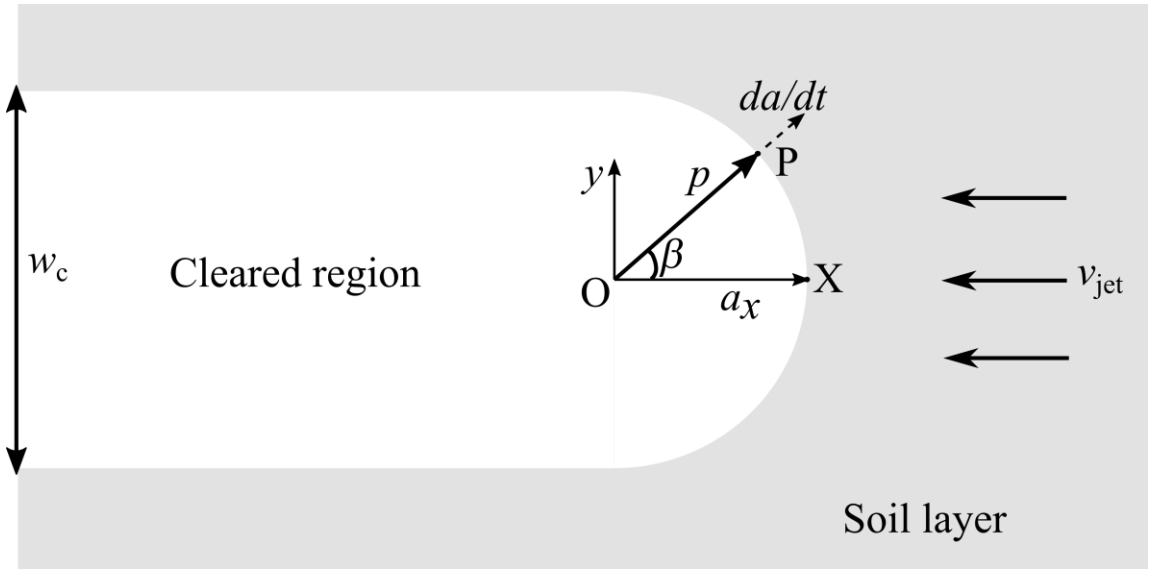

Figure 5 - Schematic (plan view) of the region cleaned by a perpendicular jet moving across a flat soiled substrate at velocity v_{jet}. The frame of reference is reversed so that soil is moved towards the jet impingement point.

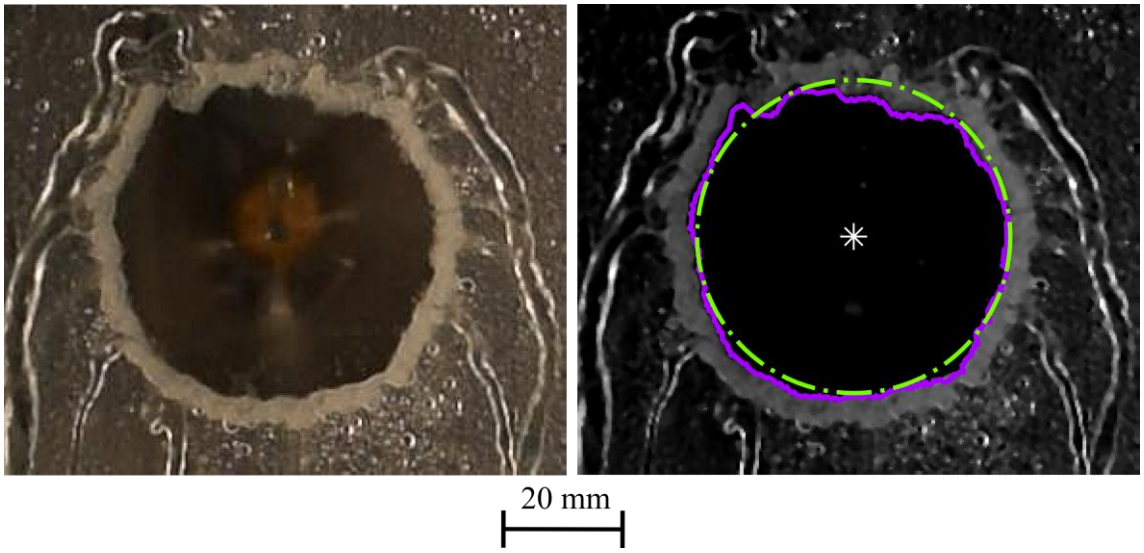

Figure 6 - Crater formed after impinging a petroleum jelly layer of thickness $\delta_o = 0.33 \pm 0.03$ mm for 514 s with Q=2.0 L min^{-1}. (a) Photograph; (b) Treated image showing the impinging point (white star), the detected border of the cleaned region (continuous purple line) and the circle with equivalent radius a (dash-dotted green circle).

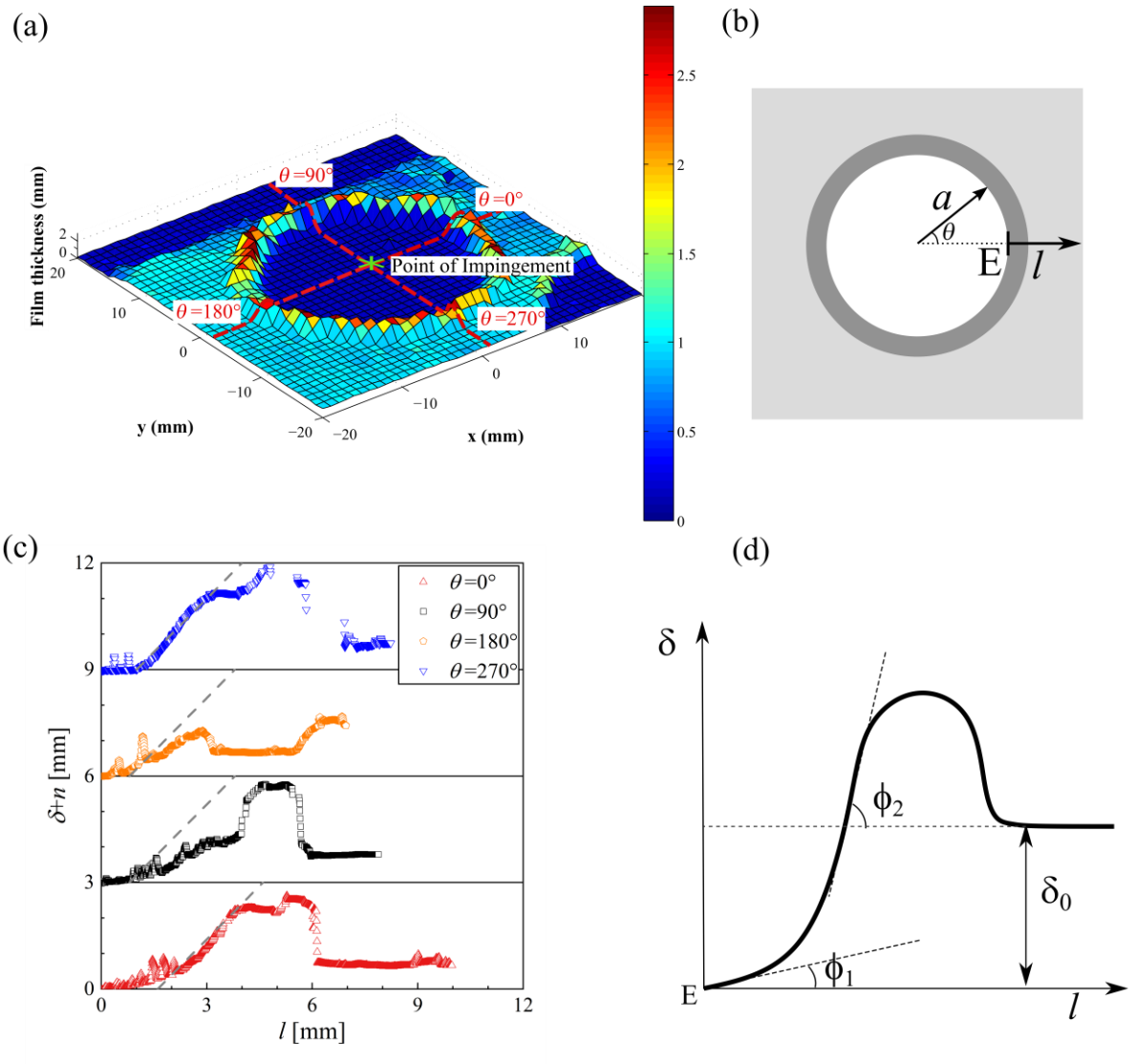

Figure 7 – Example of profilometry of the soil layers after cleaning. (a) three-dimensional scan of the crater for $Q = 2$ L/min; $\delta_o = 0.86$ mm; t =0.5 s; $\Delta x = \Delta y$ =1 mm; (b) – Coordinates used to describe the shape of the rim in (a); (c) Profiles of the crater in (a). The vertical axis is the thickness of the layers scanned at the four values of θ, shifted to aid visualization of the data. The horizontal coordinate shows the distance l from the edge of the rim, E, and the grey dashed lines represent an inclination of 45º plotted as a guide to the eye. (d) schematic representation of the shape of the dislodged rim: the angles ϕ_1 and ϕ_2 are indicated

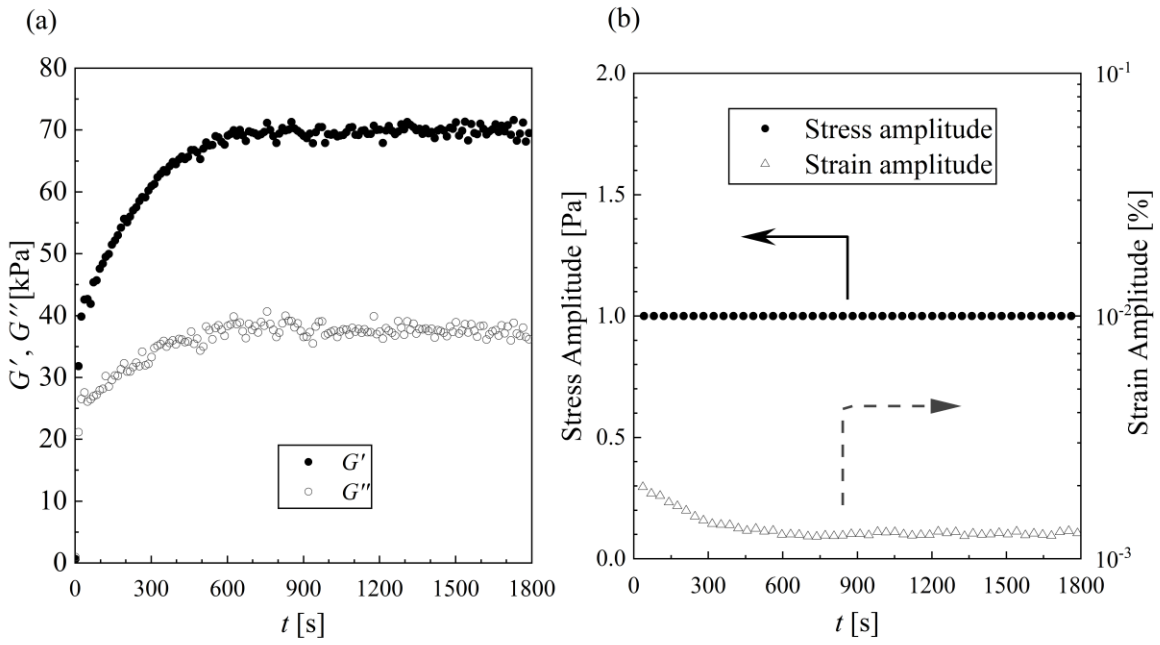

Figure 8 – Oscillatory rheometry of the petroleum jelly. (a) Dynamic moduli (G' and G'') as a function of time for a low amplitude oscillatory time sweep with constant stress amplitude. (b) Stress and strain amplitudes for the experiment in (a), indicating that the response is in the linear viscoelastic regime

785

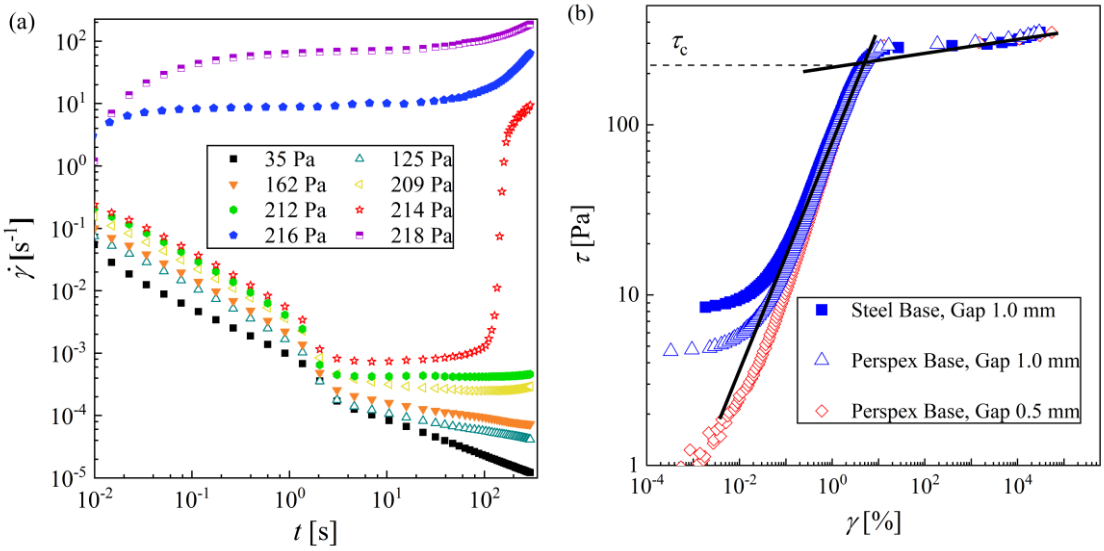

Figure 9 – Shear rheometry of petroleum jelly. (a) Evolution of shear rate for creep tests, roughened parallel plates. (b) Shear stress as a function of shear strain for shear stress ramps conducted with steel and Perspex™ bases.

790

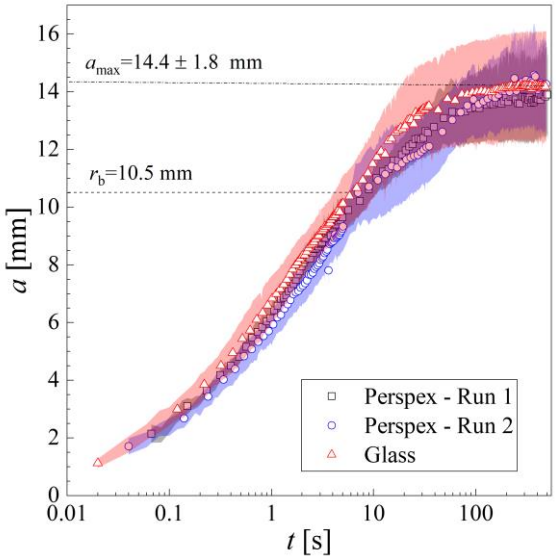

Figure 10 – Evolution of the cleaned radius for three repetitions of the experiment with $Q =$ 1 L/min, $\delta_o = 0.37 \pm 0.02$ mm conducted on Perspex™ and glass plates. Shaded regions represent the standard deviation of the data.

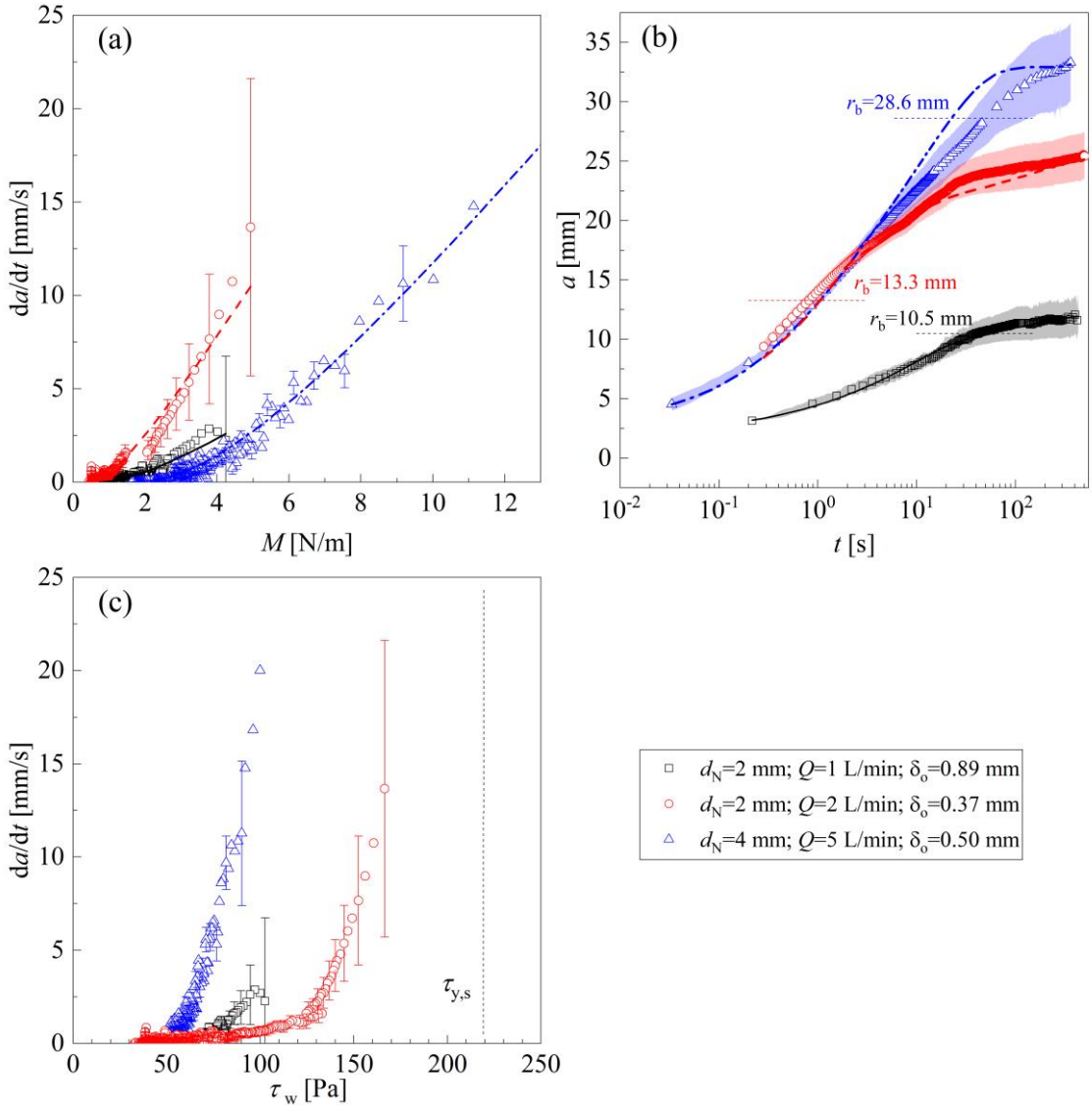

Figure 11. Effect of flow rate on cleaning performance. (a) da/dt as a function of M for three cleaning experiments: M calculated using Eq. [18]. Error bars represent the propagated uncertainty in da/dt and lines represent the fit of Eq. [32a]. (b) Evolution of cleaned radius a over time for the experiments in (a). Lines indicate the integration of Eq. [32a]. (c) da/dt vs τ_w for the experiments in (a).

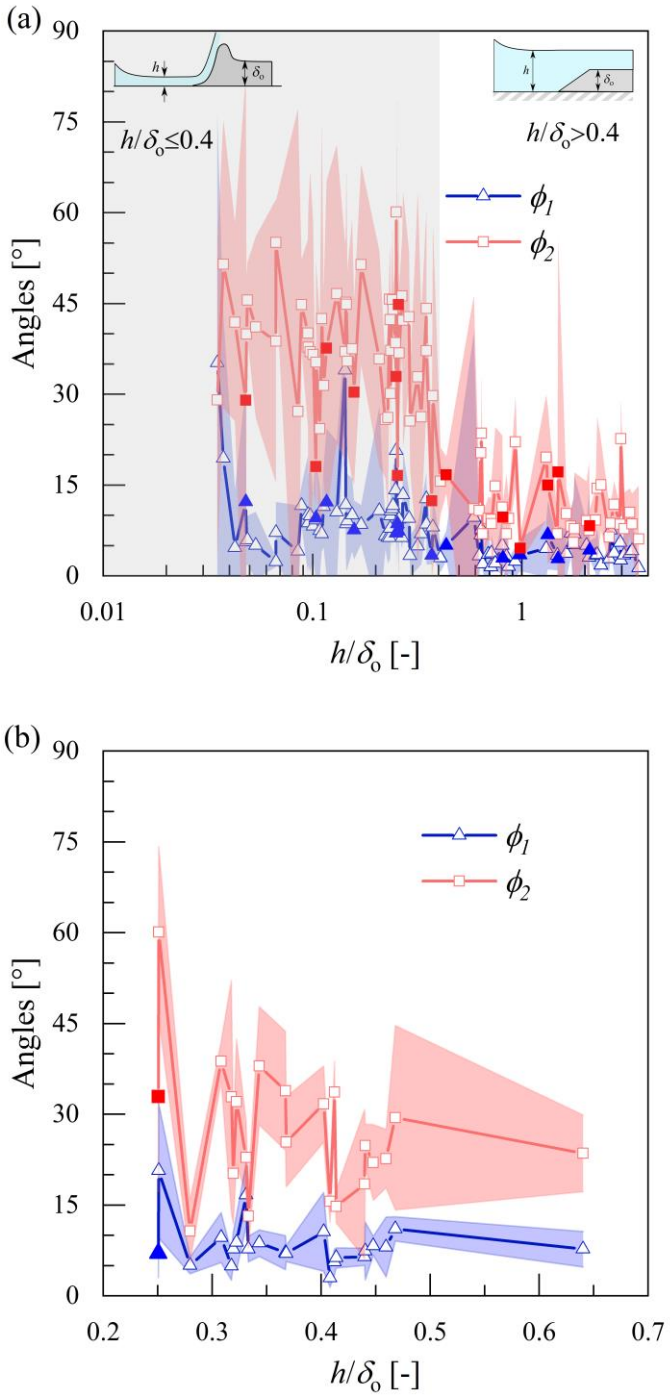

Figure 12 Summary of cleaning front shapes. (a) Effect of h/δ_o on ϕ_1 and ϕ_2 for cleaning experiments conducted with different flow rates, $d_N = 2$ mm. Solid symbols indicate experiments that were run until approaching a_{max}.Two regimes are evident: for $\frac{h}{\delta_o} \leq 0.4$, $\phi_2 \approx 45°$ and $\phi_2 > \phi_1$. For $\frac{h}{\delta_o} > 0.4$, $\phi_2 \approx \phi_1$. (b) Evolution of angles ϕ_1 and ϕ_2 during a cleaning test: experiment with $d_N = 2$ mm, $Q = 1$ L/min, $\delta_o = 0.37$ mm interrupted at different stages and angles measured. Shaded areas represent the 95% confidence interval of the measurements in the four cardinal directions.

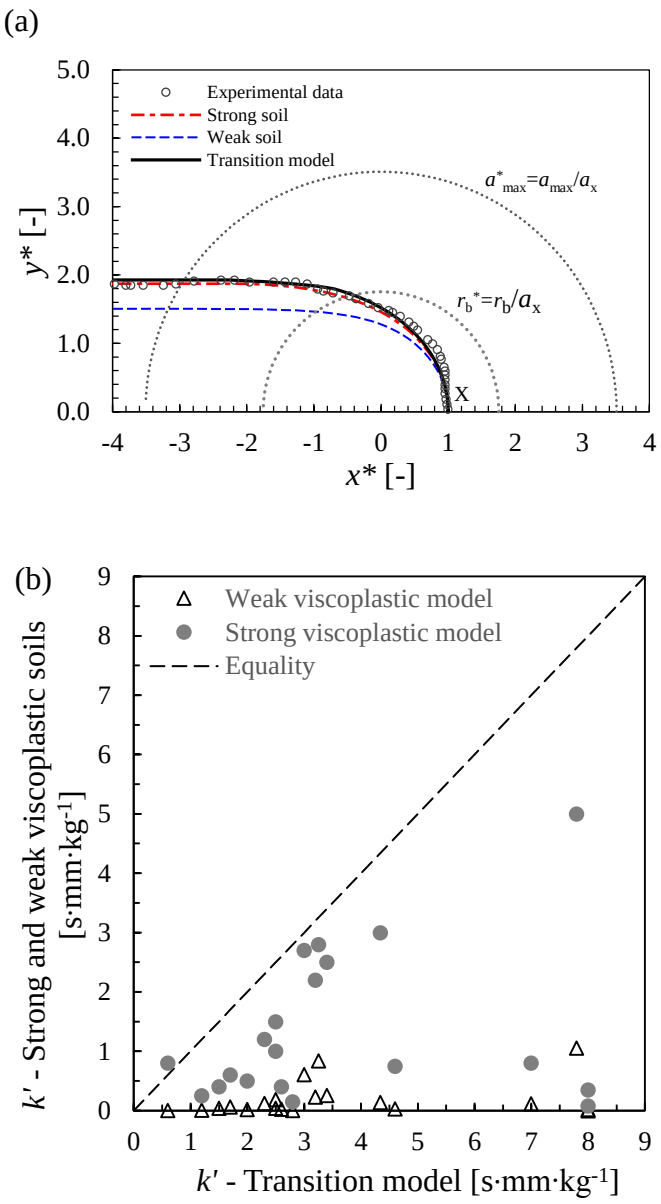

Figure 13 – Cleaning by a traversing jet. (a) Half-width of the trail generated by a moving jet with $d_N = 2$ mm; $Q = 2$ L/min; $\delta_o = 0.33$ mm; and $v_{jet} = 15.09\ mm/s$. Fits of the strong viscoplastic soil, weak viscoplastic soil and transition model are shown. Dotted lines denote the *loci* of r_b/a_x and a_{max}/r_b. (b) k' found by fitting the strong and the weak viscoplastic soil models as a function of k' found by fitting the transition model. Dashed line denotes the line of equality.

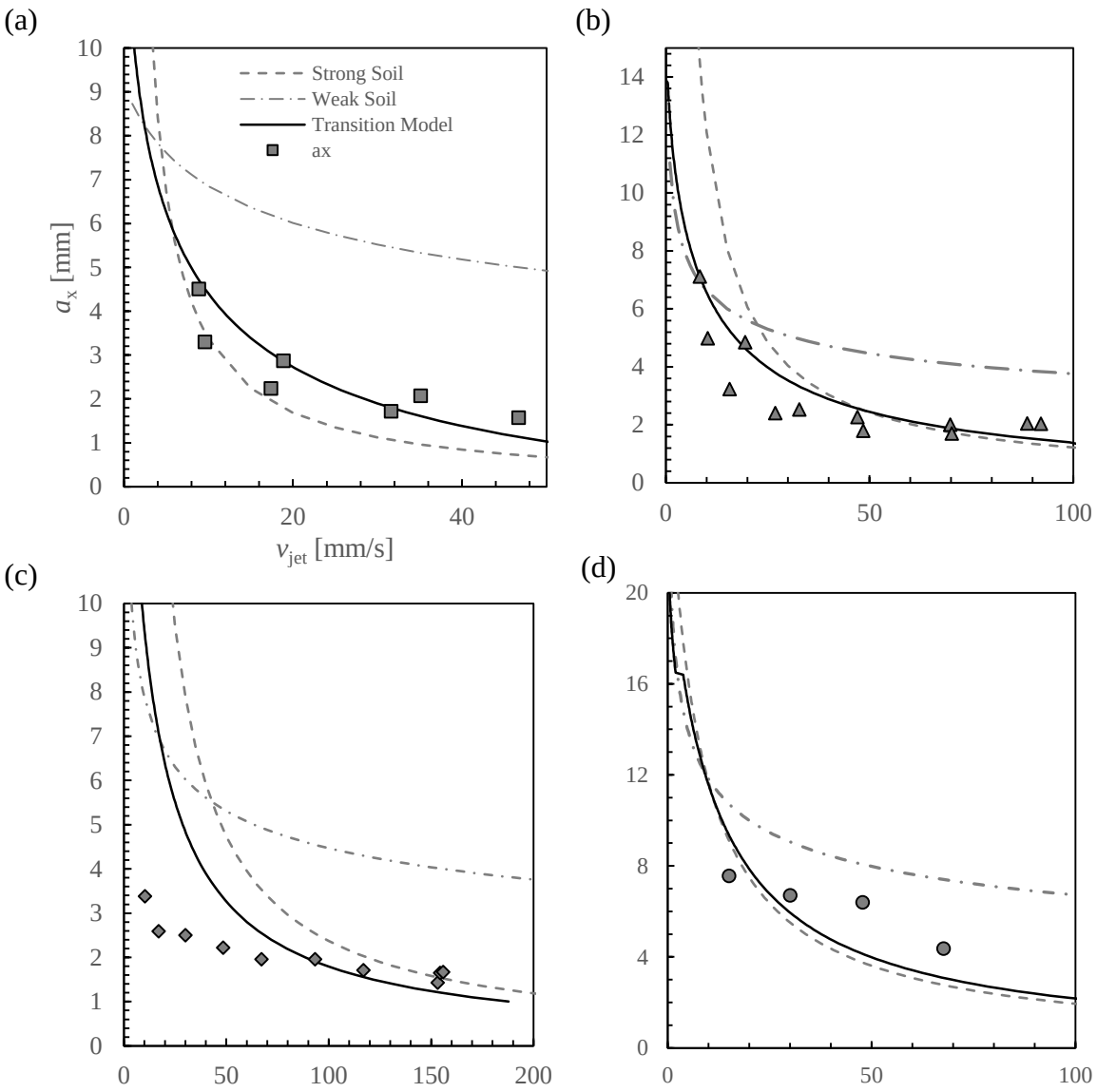

825 Figure 14 Traversing jet: effect of v_{jet} on a_x and w_{c}. $d_{\mathrm{N}} = 2$ mm: (a) $Q = 1$ L/min, δ_{o}=0.606 mm; (b) Q=1.2 L/min, , δ_{o}=0.382 mm; (c) $Q = 1.6$ L/min, δ_{o}=0.606 mm and (d) $Q = 2$ L/min, δ_{o}=0.333 mm. Lines denote the results of the strong viscoplastic, weak viscoplastic and transition models, symbols denote the experimental values of a_{x}.

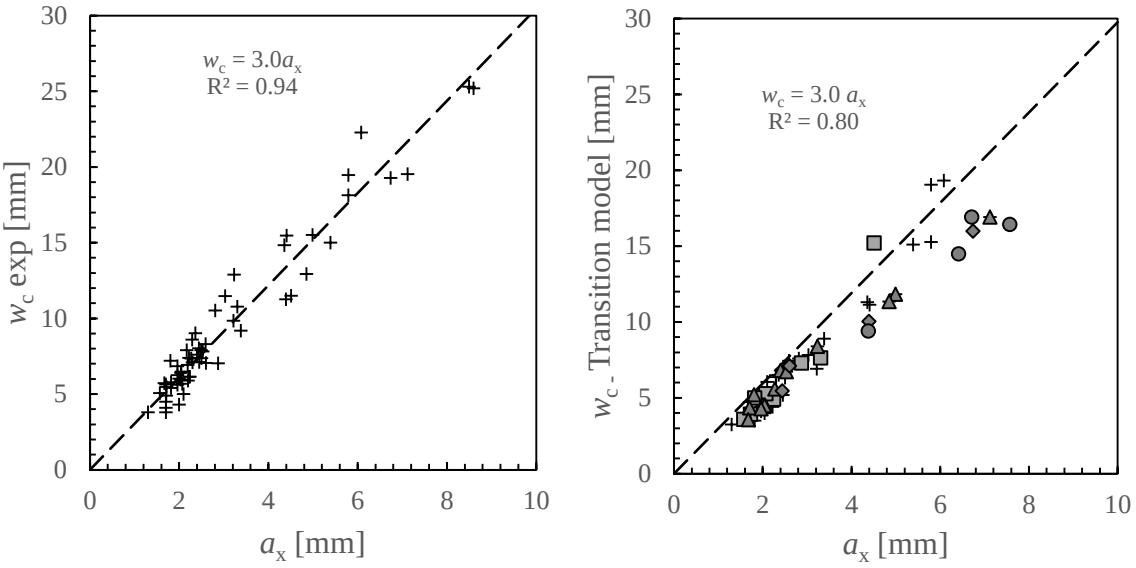

830

Figure 15 - w_c as a function of a_x for the moving jet experiments: (a) w_c measured from image analysis in the experiments, (b) w_c found by fitting the transition model. Symbols are those used in Figure 14

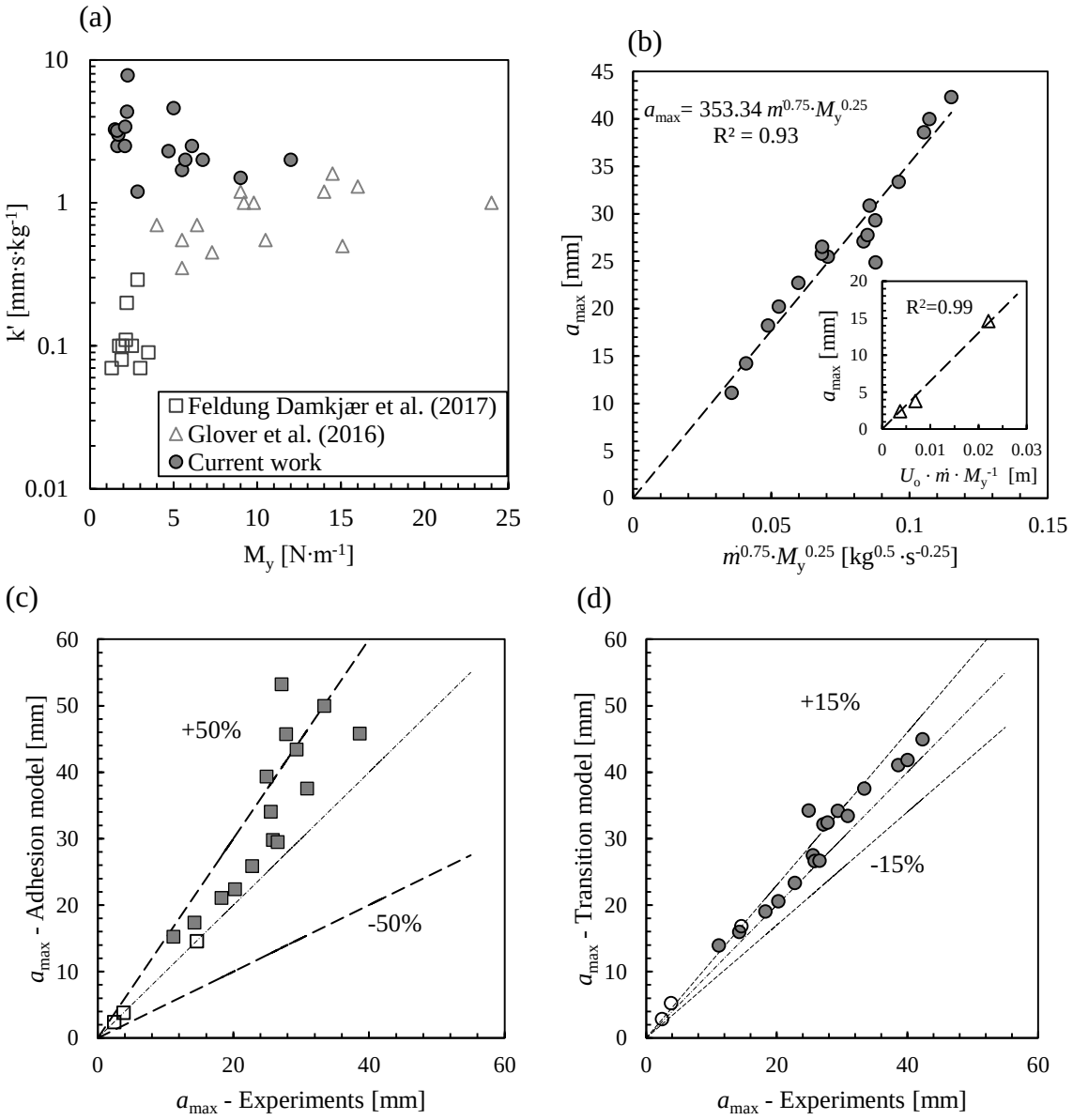

Figure 16 – Transition model parameters obtained for different studies of jet cleaning of petroleum jelly. (a) k' and M_y obtained for (*i*) the current work, (*ii*) Glover *et al.* (2016), and (*iii*) Feldung Damkær *et al.* (2017); (b) relationship between $a_{\max}$ and M_y plotted in the form suggested by Eq. [34] (weak soil). Inset shows the trend for strong soil cases (Eq. [33]). (c) agreement between $a_{\max}$ estimated with the adhesion model, Eq. [30] and [31], and experimental values. (d) agreement between $a_{\max}$ estimated with the transition model, Eq. [33] and [34], and experimental values. Solid symbols in (c) and (d) indicate cases where $a_{\max} > r_b$, open symbols $a_{\max} < r_b$.

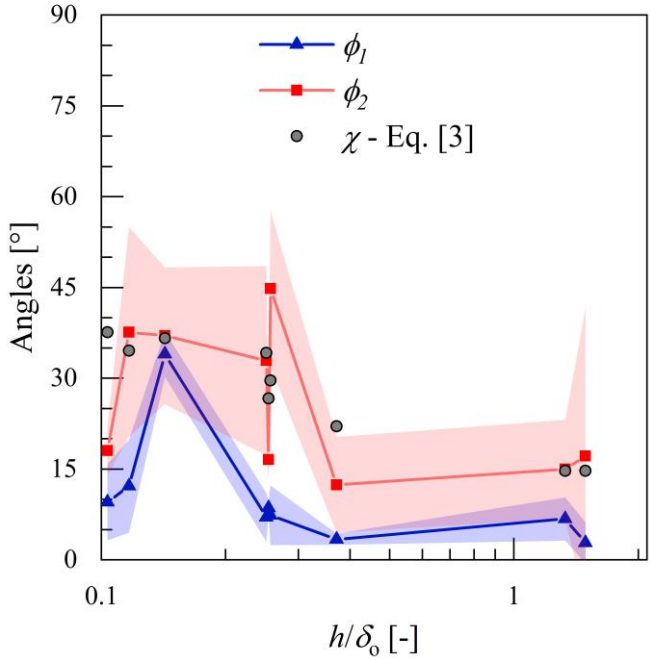

Figure 17 – Comparison of measured rim shape for the asymptotic cases with χ calculated using the wedge model of Glover *et al*. (Eq. 3) : angles ϕ_1 and ϕ_2 are the asymptotic cases reported in Figure 12(a).

850

Appendix: Identifying the form of the transition model, Eq. [32]

Figure 2 shows the trend observed in the experimental data. The expression needs to capture the linearity at large M and da/d$t \rightarrow 0$ as $\mathrm{M} \rightarrow 0$. It is desirable to minimise the number of fitting parameters. Two candidates considered were

(i) Addition of a first order decay smoothing term, *viz*

$$\frac{da}{dt} = k'\left[\left(M - M_{\mathrm{y}}\right) + M_{\mathrm{y}}\exp\left(-\frac{M}{M_{\mathrm{y}}}\right)\right] \qquad [A.1]$$

$$= k' M_{\mathrm{y}}\left[\left(\frac{M}{M_{\mathrm{y}}} - 1\right) + \exp\left(-\frac{M}{M_{\mathrm{y}}}\right)\right]$$

(ii) Addition of a quadratic smoothing term

$$\frac{da}{dt} = k'\left[M - M_{\mathrm{y}}\left(\frac{M}{M + M_2}\right)^2\right] \qquad [A.2]$$

where M_2 is a constant to be defined. Observation of asymptotic behaviour (*i.e.* da/dt = 0 at $a_{\max}$, with $M > 0$) requires that

$$1 - M_y\frac{M}{(M + M_2)^2} = 0 \qquad [A.3]$$

This has one real root, at $M_2 = M_y/4$. When $M_2 < \frac{M_y}{4}$ it can be shown that Eq. [A.2] remains positive but passes through a maximum, which is infeasible, so the function is truncated, giving

$$\frac{da}{dt} = k' M_{\mathrm{y}}\left[\frac{M}{M_{\mathrm{y}}} - \left(\frac{\frac{4M}{M_{\mathrm{y}}}}{\frac{4M}{M_{\mathrm{y}}} + 1}\right)^2\right] \qquad M/M_{\mathrm{y}} > \tfrac{1}{4} \qquad [A.4]$$

$$\frac{da}{dt} = 0 \qquad M/M_{\mathrm{y}} \leq \tfrac{1}{4}$$

The two expressions are compared in Figure A.1

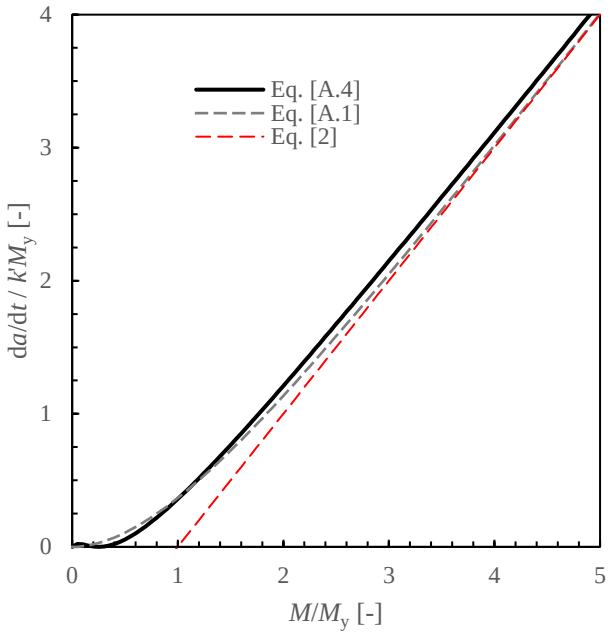

865

Figure A1 – Candidates for the transition model: Eq. [A.4] and Eq. [A.1] are plotted alongside Eq. [2], the adhesive removal model.